國 立 交 通 大 學

電信工程學系

碩 士 論 文

應用於多輸入多輸出無線通訊之高效率
瑞立衰減通道模擬器

Efficient Rayleigh Fading Channel Simulators for

MIMO Wireless Communications

研 究 生：黃姿璇　　　　　Student: Tzu-Hsuan Huang

指導教授：李大嵩 博士　　　Advisor: Dr. Ta-Sung Lee

中 華 民 國 九 十 七 年 六 月

應用於多輸入多輸出無線通訊之高效率 瑞立衰減通道模擬器

Efficient Rayleigh Fading Channel Simulators for MIMO Wireless Communications

研 究 生：黃姿璇　　　　　　Student: Tzu-Hsuan Huang

指導教授：李大嵩 博士　　　　Advisor: Dr. Ta-Sung Lee

國立交通大學

電信工程學系碩士班

碩士論文

中 華 民 國 九 十 七 年 六 月

應用於多輸入多輸出無線通訊之高效率
瑞立衰減通道模擬器

學生：黃姿璇　　　　　　　　　指導教授：李大嵩 博士

國立交通大學電信工程學系碩士班

摘要

在多輸入多輸出衰減通道中，其子通道具相關性，這成為多天線系統及空間-時間技術中效能估算的主要關鍵。在分析通訊系統中，一般都將通道假設為廣義平穩非相關散射通道。基於廣義平穩非相關散射通道所設計之通道衰減模擬器，一般而言具有高準確性。此外，因通道是操作在高取樣頻率下，若欲實現一個即時的通道模擬器則通道衰減模擬器應具有低計算複雜量；因此，如何實現一個正確且快速的模擬器成為一個重點的議題。在本論文中，吾人使用 KL 展開法提出一個高效率的衰減通道模擬器。比起既有使用弦波疊加的方法，此模擬器可有效增進通道統計特性的正確性且需要較低的計算複雜量。最後，從模擬的結果証實吾人所提出的衰減通道模擬器符合即時多輸入多輸出通道的需求。

Efficient Rayleigh Fading Channel Simulators for MIMO Wireless Communications

Student: Tzu-Hsuan Huang   Advisor: Dr. Ta-Sung Lee

Department of Communication Engineering

National Chiao Tung University

Abstract

Simulation of multiple-input multiple-output (MIMO) fading channels, with correlated subchannels is the key to performance evaluation of space-time techniques in multi-antenna systems. Wide sense stationary uncorrelated scattering (WSS-US) channels are assumed for the analysis of communication system. The fader is typically designed under the assumption of WSSUS channels, which is shown to exhibit high accuracy. Furthermore, since the channel is operated at a high sampling rate, low computational complexity is essential if a real-time channel simulator is desired. Therefore, how to realize an accurate and fast channel model becomes an important issue. In this thesis, we propose an efficient fading channel simulator by using the K-L expansion method. It can improve the accuracy of the statistical properties of the model and requires lower computational complexity than traditional models using sum-of-sinusoids. Finally, simulation results suggest that the proposed fading channel simulator meets the demand of real-time MIMO channel.

Acknowledgement

I would like to express my deepest gratitude to my advisor, Dr. Ta-Sung Lee, for his enthusiastic guidance and great patience. I also wish to thank my friends for their encouragement and help. Finally, I would like to show my sincere thanks to my parents for their inspiration and love.

Contents

Chapter 3   Rayleigh Fading Channel Simulators for SISO System……… 33

List of Figures

List of Tables

Acronym Glossary

3GPP	third generation partnership project
AoA	angle of arrival
AoD	angle of departure
AS	angle spread
BS	base station
CIR	channel impulse response
CDF	cumulative distrivution function
DS	delay spread
IFFT	inverse fast fourier transform
ISI	inter-symbol interference
K-L	Karhunen-Loeve
LOS	line-of-sight
LS	least square
MIMO	multiple-input multiple-output
MSE	mean square error
MS	mobile station
NLOS	non-line-of-sight
PAS	power azimuth spectrum
PDF	probability distribution function
SCM	spatial channel model

SF   shadow fading

SISO   single-input single-output

T-R   transmitter-receiver

US   uncorrelated scattering

WGN   white Gaussian noise

WSS   wide sense stationary

WSS-US   wide sense stationary uncorrelated scattering

Notations

B_D	Doppler spread
B_S	bandwidth of signal
T_S	symbol period
T_s	sampling time
T_C	coherence time
v	speed
λ	wavelength of carrier wave
λ_T	transmit antenna spacing
λ_R	receive antenna spacing
f_m	maximum Doppler frequency
w_m	maximum Doppler frequency in radius
f_c	carrier frequency of the scattered signal
C	speed of light
$g(t)$	complex faded envelope
τ	multipath delay
N	number of propagation paths of single fader
M	number of fader
L	number of main link in MIMO channel
$J_0(\cdot)$	Bessel function
$r(t)$	Wideband faded envelope
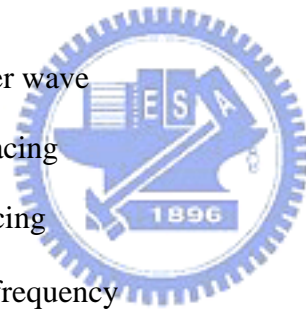
H   channel matrix

S symbol rate

Chapter 1

Introduction

In mobile radio communications, the emitted electromagnetic waves frequently do not reach the receiving antenna directly due to obstacles blocking the line-of-sight path. In fact, the received signals are a superposition of waves coming from all directions due to reflection, diffraction, and scattering caused by buildings, trees, and other obstacles. This effect is known as multipath propagation. Because of the multipath propagation, the received signal consists of an infinite sum of attenuated, delayed, and phase-shifted replicas of the transmitted signal, each influencing each other. Depending on the phase of each partial wave, the superposition may be constructive and destructive. Apart from that, when transmitting digital signals, the form of the transmitted impulse can be distorted during transmission and often several individually distinguishable impulses occur at the receiver due to multipath propagation. This kind of effect is called impulse dispersion. The extent of impulse dispersion depends on the propagation delay differences and the amplitude relations of the partial waves.

Besides the multipath propagation, the Doppler effect also has a negative influence on the transmission characteristics of the mobile radio channel. Because of Doppler effect, the spectrum of the transmitted signal undergoes a frequency expansion during transmission. This is named frequency dispersion. The extent of

frequency dispersion mainly depends on the maximum Doppler frequency and amplitudes of the received partial waves. In the time domain, the Doppler effect implies that the impulse response of the channel becomes time variant. Due to the time-variant characteristic of the impulse response, mobile radio channels can be generally regard as linear time-variant systems. Due to the Doppler effect and multipath propagation, Rayleigh fading is a statistical model for the effect of a propagation environment on a radio signal [1]-[25].

Channel simulators are operated at a high sampling rate, which will cost a lot of computation time. Thus, a fading channel simulator with low computational complexity is desired. How to realize an accurate and fast fading channel simulator thus becomes an important issue. Common methods for simulating fading channels can be classified into three types: Direct form model, modified Jakes model, and KL expansion model. In the direct form model, the channel is a discrete-time lowpass-equivalent channel impulse response, for which the concept of digital signal processing can be adopted for further modification [13]. The modified Jakes model is based on sum-of-sinusoids for simulation. Because the Jakes model [18] has a major shortcoming that the generating signals must be wide-sense-nonstationary, there are various modified versions proposed [19]-[24]. In the K-L expansion model, the number of terms needed by the truncated K-L expansion is less than traditional methods with sum-of-sinusoids.

In this thesis, we propose two methods for simulating Rayleigh fading channels. Unlike Jakes model, the proposed models are consistent with the WSS-US channel and require a lower computational complexity. The first method adopts the concept of sum-of-sinusoids like the Jakes model, and the second adopts the concept of K-L expansion and involves the approximation of Bessel function [25] to realize the fading channel. Furthermore, we propose the Chebyshev approximation to achieve further

reduction in computational loading. We compare two proposed methods and find that the model using K-L expansion method is more accurate and requires lower computational complexity. Next, the fading simulator based on K-L expansion method is extended to MIMO system via the introduction of a correlation matrix. The proposed MIMO channel simulator is demonstrated by computer simulations to be consistent with realistic environment.

The thesis is organized as follows. In Chapter 2, we introduce fading models and WSS-US channels. In Chapter 3, the proposed Rayleigh fading simulators with a single fader are developed. In Chapter 4, the fading simulator is extended to MIMO systems. Finally, Chapter 5 gives the conclusion.

Chapter 2

Mobile Radio Propagation Channel Models

The propagation properties of mobile radio propagation channel can be classified into three categories: reflection, diffraction, and scattering, which can be shown in Figure 2-1 [2]. Reflection is the change in direction when a wave front strikes a surface between two different media, so the wave front direction returns into the original medium. This phenomenon occurs when the surface is larger than the wavelength of incident wave. Diffraction happens according to Huygen's principle while an obstruction is existed between the transmitter and receiver antennas, so the secondary waves are produced behind the obstruction. Scattering arises when the plane wave is incident upon an object and causes the energy to be redirected in many directions.

In virtue of the above three properties, the phenomenon of mobile radio propagation can be roughly represented as three nearly independent classes: path loss, slow log-normal shadowing effect, and fast multipath fading. Each phenomenon is induced by the distinct physical principle and each must be specified while designing and evaluating the performance of the cellular network.

As a consequence of reflections, diffractions and scatterings, multiple waves arrive at a mobile station (MS) by diverse propagation delay and from various

directions. The characteristic is thought as multipath propagation. The scatters of multipath propagation can be divided into three groups: local-to-mobile scatters, local-to-base scatters, and remote scatters as shown in Figure 2-2. Local-to-mobile scatters induce Doppler spread by buildings around MS. Local-to-base scatters induce angle spread by buildings around base station (BS). Remote scatters cause delay and angle spread by terrain features or high-rise buildings between BS and MS.

Considering a carrier signal transmitted in the multipath environment, the small changes in the distinctive delays by MS mobility will induce large changes in the phases of the arriving plane waves. Constructive and destructive additions of arriving plane waves reveal themselves as large variations in the phase and amplitude of the combined received signal. Because of the mobility at MS, the spatial variations in the envelope and phase of the combined received signal represent themselves as time variations. The phenomenon is called envelope fading whose rate depends on the velocity of the MS.

The directions of arriving plane waves may be significant different. A MS in the microcellular environment is usually surrounded by local scatters, so that the plane waves will arrive from different directions sometimes without line of sight (LOS) components. The assumption at MS is modeling as isotropic scattering which the plane waves arrive from all direction with equal probability. In the other hand, the BS antennas are only moderately evaluated above the local scatters.

Sometimes, multipath-fading is called as fast fading with short-term signal variations for distinguishing it from shadowing effect, which exhibits itself as the long-term signal variations of the mean envelope over the distance. The difference can be showed in Figure 2-3. Path loss predicts the transmitted power decays with distance from a BS. The researches proposed by Hata [3] and Okumura [4] incurred path loss models for microcellular systems. The models can be fit in all environments

5

like urban, suburban, and rural areas. Recently, the works of path loss model for microcellular systems have been suggested. The COST231 [5] model was proposed for urban areas and microcellular systems.

Diffraction by big structures

Mobile

Basestation

Reflection by a smooth surface

Scattering by a rough surface
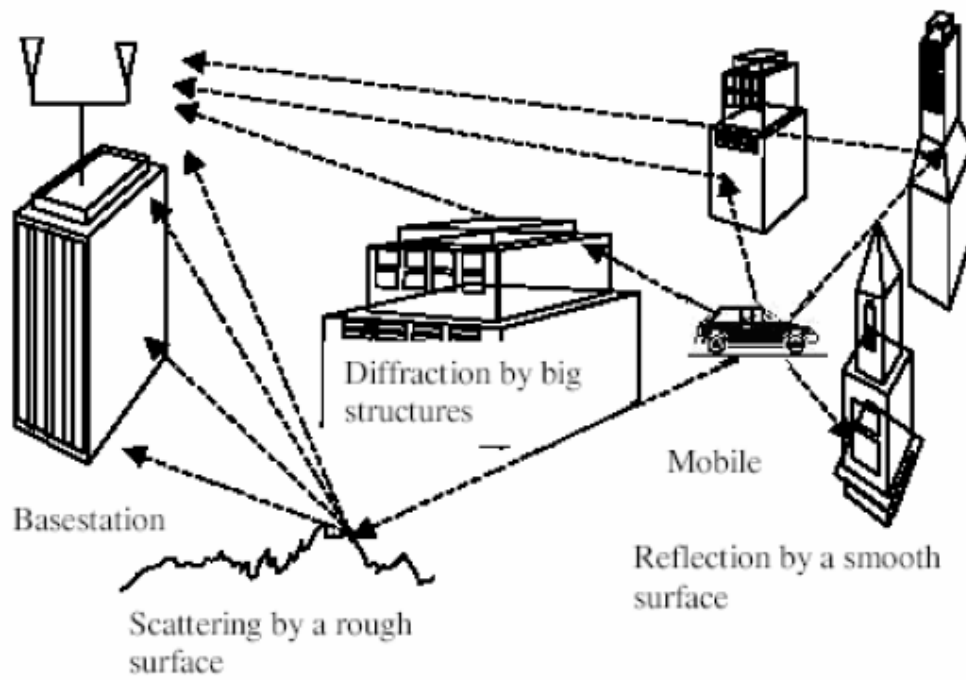
Figure 2-1: Propagation properties of mobile radio channels
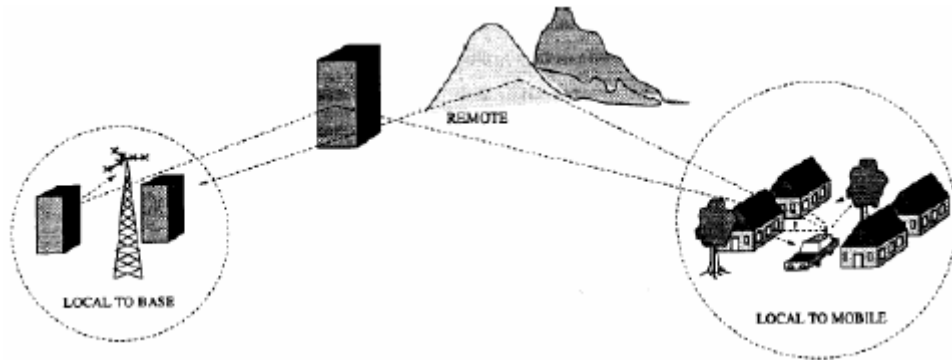
Figure 2-2: Scatters of Multipath propagation
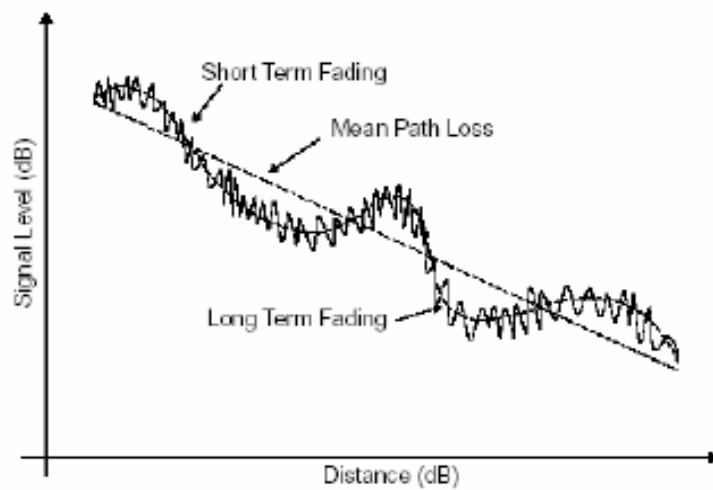
Figure 2-3: Long-term fading and short-term fading

2.1 Large Scale Propagation Model

Large scale fading caused by shadowing effects or natural features is also called large scale fading. Typically, it is modeled by using log-normal distribution in signal level. When the coherence time of the channel is relatively large to the delay of the channel, large scale fading arises. The amplitude and phase varied by the channel can be thought as constant over the period. The attenuation of transmitted signal power for received signal can be predicted by propagation models. Propagation models which predict the mean signal strength for an arbitrary transmitter-receiver (T-R) separation distance are of great use to predict the coverage area of transmission. Propagation models are divided into three types: free space model, path loss model, and path loss model with shadowing. We will introduce these types in the following section.

2.1.1 Free Space Model

The free space model is used to predict the received signal strength when the propagation environment is clear, unobstructed line-of-sight (LOS). There are several applications such as Satellite and microwave line-of-sight radio link for free space model. We can model the free space model by using Friis free space equation:

$$P_r(d) = \frac{\lambda^2}{(4\pi)^2 d^2 L} \cdot G_t \cdot G_r \cdot P_t \tag{2-1}$$

where P_t is the transmitted power, $P_r(d)$ is the received power which is a function of separation distance, G_t and G_r are the transmitter and receiver antenna gain respectively, d is the T-R separation distance, λ is the carrier wavelength, and L is the system loss factor with constrained condition: $L \geq 1$. The factor L is affected by transmission line attenuation, filter losses, and antenna losses. For the special case of $L = 1$, indicate no loss in the hardware of the communication system. In the free

space, the coverage is able to reach 10km per 20dB decay [6].

2.1.2 Path Loss Model

For common wireless communications, the relationship of transmitted path loss and T-R separation can be expressed as [7]:

$$PL(d) \propto \left(\frac{d}{d_0}\right)^n$$
(2-2)

The relationship can be reformulated as:

$$\overline{PL}(\text{dB}) = PL(d_0) + 10n \log\left(\frac{d}{d_0}\right)$$
(2-3)

where $\overline{PL}$ is the average path loss, d is the T-R separation distance, n is the path loss exponential which is related to the measurement environment listed in Table 2-1 [8], and d_0 is the reference distance. Typically, the value of d_0 is referred as 1 km for large cells, 100 m for microcells, and 1 m for indoor channels. Because mobile communication system always works in the urban area, the coverage is about 10 km per 40 dB.

Table 2-1: Path loss exponential for different environments

Environment	Path Loss Exponent, n
Free space	2
Urban area cellular radio	2.7 to 3.5
Shadowed urban cellular radio	3 to 5
In building LOS	1.6 to 1.8
Obstructed in building	4 to 6
Obstructed in factories	2 to 3

Hata model is one of famous path loss models for describing the measure environment such as: urban, suburban, and rural area. The formulation of Hata model can be described as:

$$PL_{urban}(dB) = 69.55 + 26.16 \log f_c - 13.82 \log h_b$$
$$- a(h_m) + (44.9 - 6.55 \log h_b) \log d,$$

(2-4)

where f_c is the carrier frequency which is valid from 150 MHz to 1500 MHz, h_b and is the BS antenna height which is valid from 30m to 120m, h_m is the MS antenna height which is valid from 1m to 10m , and d is the T-R separation distance in kilo meters, and $a(h_m)$ is the correlation factor for effective mobile antenna height. The correlation factor $a(h_m)$ will be different from measure environments.

For small to medium city,

$$a(h_m)(\text{dB}) = (1.1 \log f_c - 0.7)h_m - (1.56 \log f_c - 0.8).$$

(2-5)

For large city,

$$a(h_m)(\text{dB}) = 8.29(\log 1.54 h_m)^2 - 1.1 \quad \text{for} \quad f_c \leq 300 \text{ MHz}$$
$$a(h_m)(\text{dB}) = 3.2(\log 11.75 h_m)^2 - 4.97 \quad \text{for} \quad f_c \geq 300 \text{ MHz}.$$

(2-6)

The Equation 2-4 is the general case, the model can modify to different measure areas and carrier frequency range. For different measure areas, the path loss model is $PL_{suburban} = PL_{urban} - 2 \log (f_c / 28)^2 - 5.4$ in the suburban area. In the open rural areas, the model is $PL_{rural} = PL_{urban} - 4.78 \log (f_c / 28)^2 - 18.33 \log f_c - 40.98$.

The formulation of Hata model extending to 2 GHz can be shown as follows:

$$PL_{urban}(dB) = 46.3 + 33.9 \log f_c - 13.82 \log h_b - a(h_m)$$
$$+ (44.9 - 6.55 \log h_b) \log d + C_M$$

(2-7)

where f_c is valid from 1500 MHz to 2000 MHz, d is the transmitted distance which is valid from 1 km to 20 km, and C_M is $0 \ dB$ for medium sized city and

suburban areas and 3 dB for metropolitan centers.

2.1.3 Path Loss Model with Shadowing Effect

The path loss model with shadowing effect is used when arriving plane wave travels through different obstructions such as buildings, tunnels, hills, trees, etc. The received signal R is described by log-normal distribution, for $r > 0$:

$$p\left(r\right) = \frac{1}{\sqrt{2\pi}\sigma r}e^{-\left(\ln r - m\right)^2/2\sigma^2},$$ (2-8)

where m and σ are the mean and standard deviation of the logarithm of the variable r.

Therefore, the path loss model with shadowing effect could be expressed in terms of $\overline{PL}$ plus a random variable X_σ, as follows:

$$\begin{aligned}\widehat{PL} &= PL\left(d_0\right) + 10n\log\left(\frac{d}{d_0}\right) + X_\sigma \\ &= \overline{PL} + X_\sigma,\end{aligned}$$ (2-9)

where X_σ is denoted as a zero-mean Gaussian distribution random variable (dB) with standard deviation 4-10 dB. The choice of X_σ is based on measurement environment.

2.2 Small Scale Propagation Model

Small scale fading is used to illustrate the rapid fluctuation of the amplitude of a radio signal over a short time period, so large-scale fading can be ignored at instant time. Fast fading is caused by multipath scattering around a user and typically follows Raleigh distribution in signal envelope. The mobile radio channel is able to model as a linear filter with a time-varying impulse response [9], which can be shown in Figure 2-4. The filtering featur of the channel is induced by the summation of amplitudes and

delays of the multiple arriving plane waves at instant time.

Delay spread and coherence time are used for describing the time variation of the channel in the small-scale fading. Doppler spread is a measure of the spectral broadening induced by the variation of time rate in the mobile radio channel. It is defined as the range of frequencies over that the received Doppler spectrum is essential non-zero. In the other hand, coherence time is the time domain in opposition to Doppler spread and is used to depict the time variation of the frequency dispersive nature in the channel. It is defined as a statistical measure of the time duration over that the channel impulse response is virtually invariant.
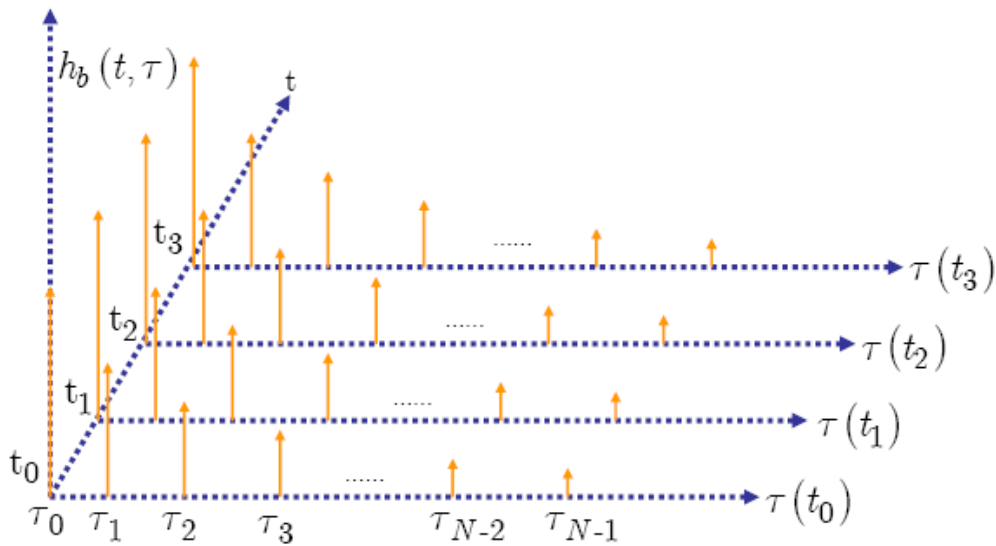
Figure 2-4: Time-varying impulse model for a multipath radio channel

2.2.1 Flat Fading vs. Frequency-Selective Fading

The channel model is classified mainly based on multipath time delay spread. If bandwidth of signal B_S is smaller than bandwidth of channel B_C $(B_S < B_C)$ and delay spread σ_τ is smaller than symbol period T_S $(\sigma_\tau < T_S)$, then the model

is called flat fading channel. On the contrary, if $B_S > B_C$ and $\sigma_\tau > T_S$ then the model is called frequency-selective fading channel. The flat fading channel and frequency-selective fading are also referred to as narrowband channel and wideband channel. The comparison of narrowband and wideband channel is shown in Figure 2-5.

Flat fading channel is suitable for narrowband transmission since the bandwidth of the applied signal is narrow as compared to the flat fading bandwidth of channel. It occurs when the inverse signal bandwidth (the duration of the signal) is much larger than the time spread of the propagation delays. Under the circumstance, the total frequencies of the transmitted signal will meet the same random attenuation and phase shift. The channel induces less or even no distortion for the received signal. The mobile radio channel experiences the constant gain and linear phase response over the bandwidth greater than the bandwidth of the transmitted signal. It can be shown in Figure 2-6.
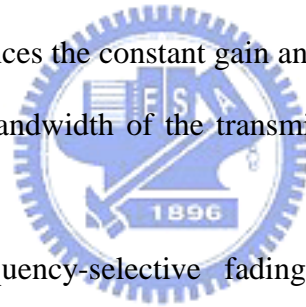
In the opposition, frequency-selective fading channel used for wideband transmission occurs when the propagation delay is larger than the inverse signal bandwidth. The transmitted signal can meet different phase shifts as the distinctive propagation delays become larger. Under the circumstance, amplitude and phase distortion are introduced by the channel for the received signal. The mobile channel owns a constant gain and linear phase response over the bandwidth of the transmitted signal. It can be shown in Figure 2-7. Frequency-selective fading is due to the time dispersion of the transmitted signal, so the channel induces intersymbol interference (ISI).
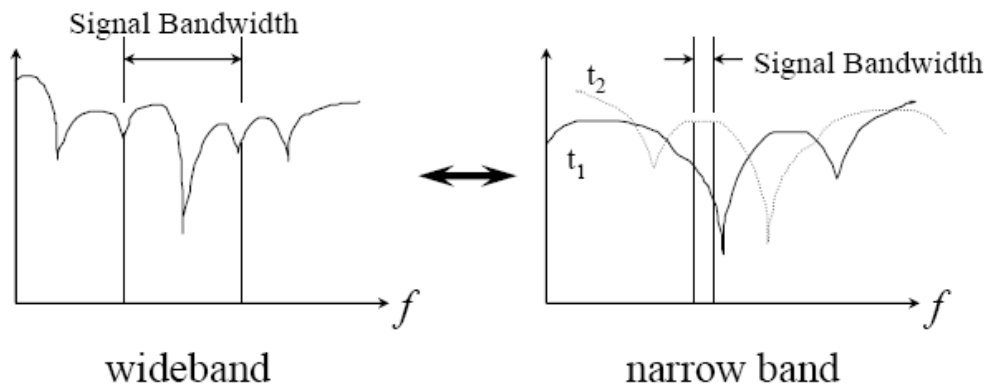
Figure 2-5: Wideband channel and narrowband channel
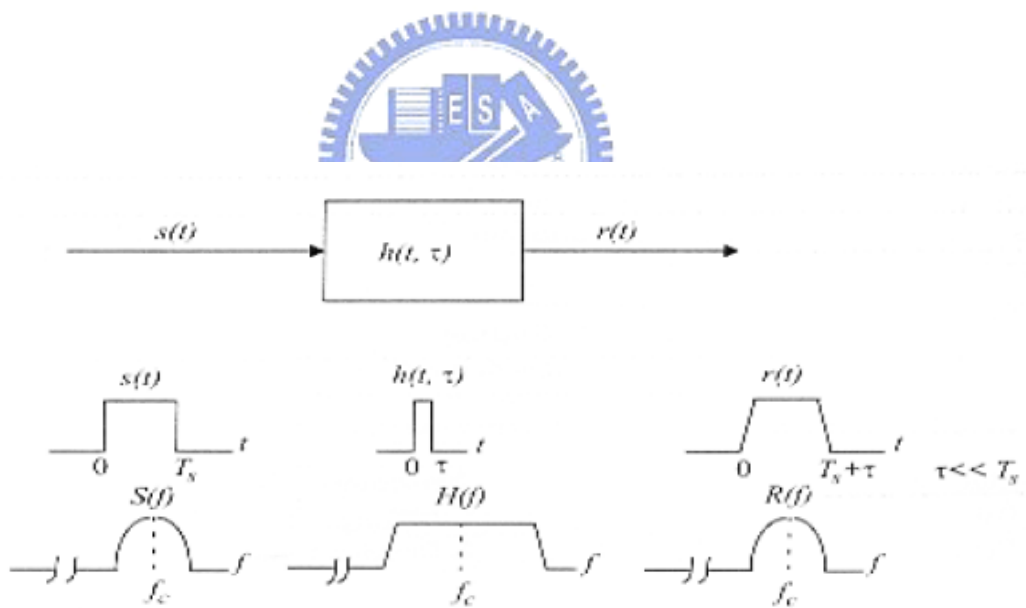
Figure 2-6: Flat fading channel characteristics
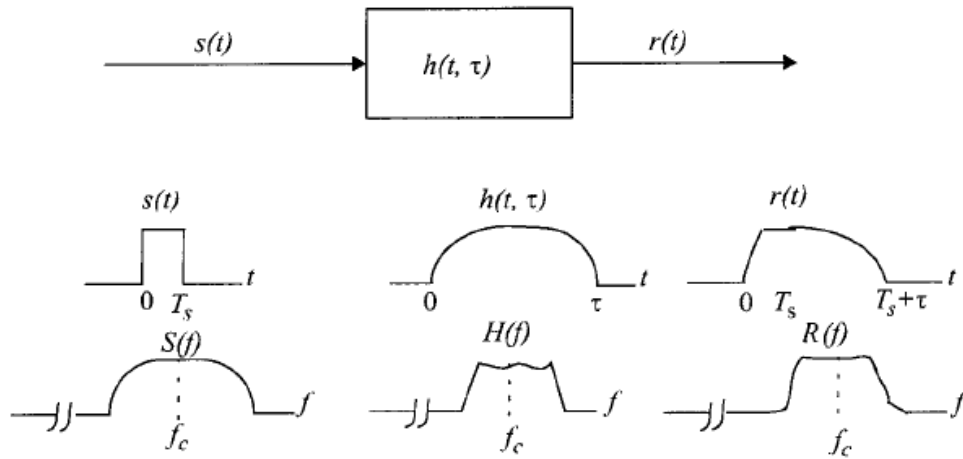
Figure 2-7: Frequency-selective fading channel characteristics

2.2.2 Fast Fading vs. Slow Fading

The channel model is classified mainly based on Doppler spread. In other words, the channel is depending on how rapidly the transmitted baseband signal changes as compared to the rate of the channel variation. If Doppler spread B_D is larger than bandwidth of signal B_S $(B_D > B_S)$ and symbol period T_S is larger than coherence time T_C $(T_S > T_C)$, then the model is called fast fading channel. On the contrary, if $B_S > B_D$ and $T_S < T_C$ then the model is called slow fading channel. It should be noted it will not specify whether the channel is flat fading or frequency-selective fading when channel is specified as fast or slow fading.

For the case of fast fading channel, the channel impulse response changes rapidly within the symbol duration of the transmitted signal. This causes signal distortion due to fast fading increasing Doppler spreading relative to the bandwidth of the transmitted signal, which leads to signal distortion. Fast fading only deals with the variational rate of the channel due to motion of BS [10]. For the case of the flat fading channel, it can simplify the impulse response to be the delta function. Therefore, the

flat and fast fading channel is a channel in which the amplitude of the delta function varies faster than the variational rate of the transmitted baseband signal. In the other case, the frequency-selective and fast fading channel is a channel in which the amplitudes, phases, and time delays of each multipath component vary faster than the variational rate of the transmitted baseband signal. It comes to a conclusion that fast fading only happens for very low data rates.

In the case of slow fading channel, the rate of changes of channel impulse response is slower than the transmitted signal. At this situation, the channel may be assumed to be static over one or several reciprocal bandwidth intervals. At view of frequency domain, it implies that the Doppler spread of the channel is much less than the bandwidth of the transmitted baseband signals [11].

The velocity of the mobile and the baseband signaling determines whether a signal undergoes fast or slow fading. For the summary, types of small-scale fading and their characteristics are shown in Figure 2-8 and Figure 2-9.

Small-Scale Fading

(Based on multipath time delay spread)

Flat Fading

1. BW of signal < BW of channel

2. Delay spread < Symbol period

Frequency-selective Fading

1. BW of signal > BW of channel

2. Delay spread > Symbol period

Small-Scale Fading

(Based on Doppler spread)

Fast Fading

1. High Doppler spread

2. Coherence time < Symbol period

3. Channel variations faster than baseband signal variations

Slow Fading

1. Low Doppler spread

2. Coherence time > Symbol period

3. Channel variations slower than baseband signal variations

Figure 2-8: Types of small-scale fading
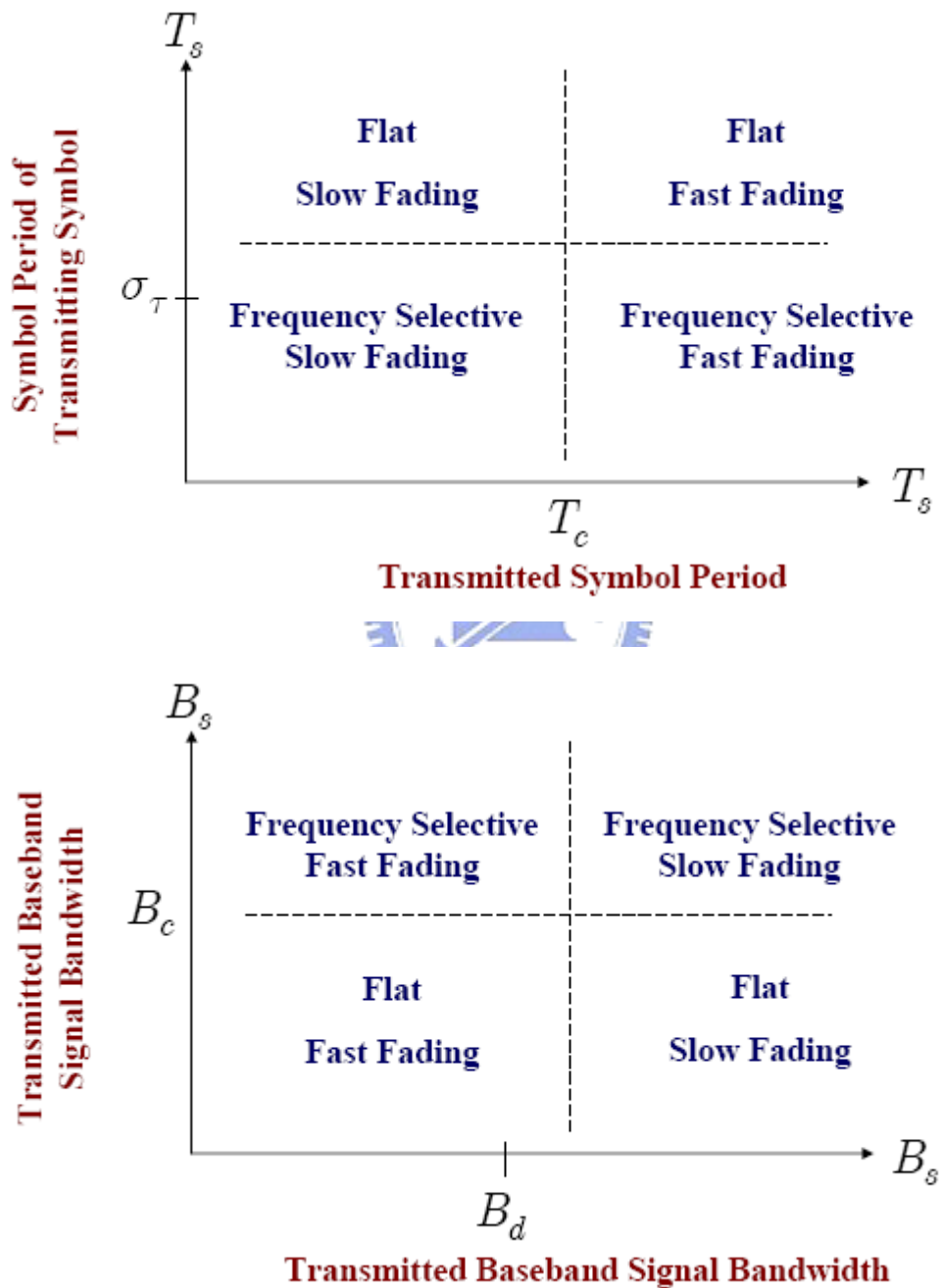
Figure 2-9: Classification of small-scale fading

2.2.3 Doppler's Effect

In the wireless mobile communications, the angles of arriving plane wave are different with the direction of movement of BS occurred by transmitter, receiver, and environment mutually shift. The phenomenon is called Doppler spread, also called Doppler shift.

The receiving antenna is move along the path with speed v from X to Y which can be shown in Figure 2-10, and the distance between X and Y is d. In the multipath channel, assume there are n arriving plane waves, phase of each arriving plane wave is ϕ_n, the angle difference of ϕ_n and the direction of movement of BS is α_n, time cost from X to Y is $\triangle t$, then the distance d can be derived as $d = v \cdot \triangle t$. The electric waves are transmitted from the transmitted antenna S, the angle α_n of X is almost the same as that of Y, because S is far away from X and Y. The increasing distance of transmission can be defined as $\triangle l = d \cos \alpha_n$, the relationship of phase change is derived as:

$$\triangle \phi = \frac{2\pi}{\lambda} \triangle l = \frac{2\pi v \triangle t}{\lambda} \cos \alpha_n, \tag{2-10}$$

where λ is the wavelength of carrier wave.

The Doppler shift f_m can be derived as:

$$f_m = \frac{1}{2\pi} \cdot \frac{\triangle \phi}{\triangle t} = \frac{v}{\lambda} \cos \alpha_n, \tag{2-11}$$

where λ is equal to C / f_c, C is the speed of light, and f_c is the carrier wavelength. The common Doppler spectrum is U-shaped spectrum which is shown in Figure 2-11. The maximum Doppler shift occurs as arriving angle is as the same as the direction of mobility, such as $\alpha_n = 0$, then $f_d = v / \lambda$.
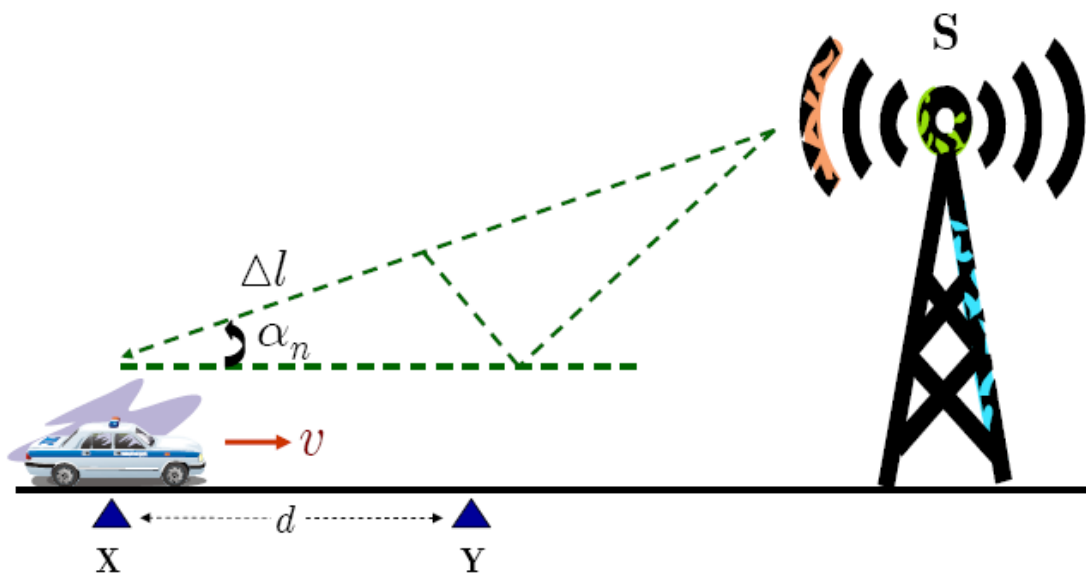
Figure 2-10: Illustration of Doppler effect
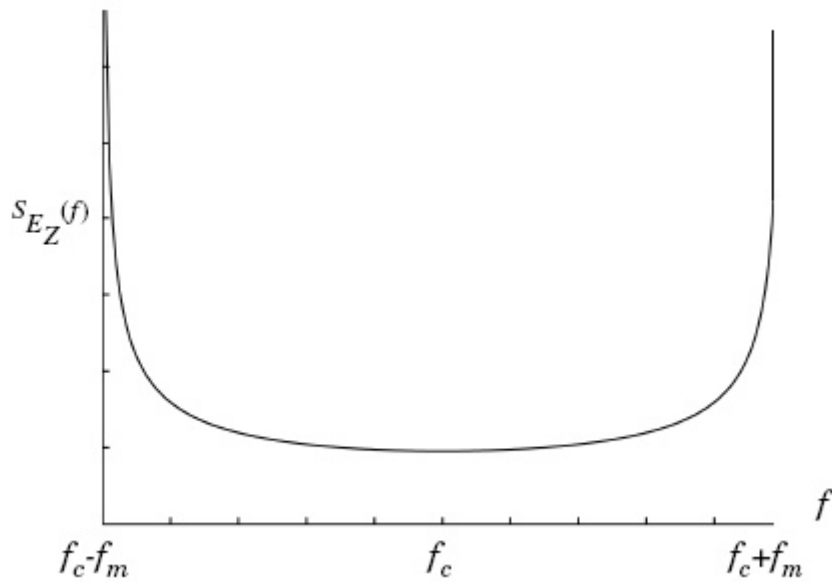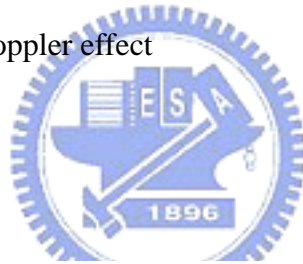
Figure 2-11: Doppler power spectrum of an unmodulated carrier signal

2.3 Rayleigh Fading in Channel Propagation

Rayleigh distribution is commonly used to describe the statistical time varying feature of the received envelope of a flat fading signal. Envelope of the sum of the two quadrature Gaussian noise signals follows Rayleigh distribution. If there is LOS component in the multipath signals, it should be modeled as Ricean distribution.

All the arriving plane waves from random scattering direction are intergraded by the receiver antenna. According to central-limit theorem and assume there are enough plane waves and no LOS components exist, the amplitudes of in-phase and quadrature phase components obey zero-mean Gaussian distribution and the phases follow uniform distribution. It is the mathematical character of Rayleigh fading channel.

Let's derive Rayleigh distribution completely. First, consider a carrier signal S with an amplitude A at a frequency w_0 :

$$S = A \exp(jw_0 t) \tag{2-12}$$

In the receiving terminal, the received signal S_r is the sum of N arriving plane waves, which can be described as

$$S_r = \sum_{i=1}^{N} a_i \exp\left[j\left(w_0 t + \theta_i\right)\right] = r \exp\left[j\left(w_0 t + \theta\right)\right] \tag{2-13}$$

where r is the envelope of receiving signal and θ is the random phase. We can define the term $r \exp(j\theta)$ in Equation (2-13) to be

$$r \exp(j\theta) = \sum_{i=1}^{N} a_i \cos \theta_i + j \sum_{i=1}^{N} a_i \sin \theta_i = x + jy \tag{2-14}$$

where $x = \sum_{i=1}^{N} a_i \cos \theta_i = r \cos \theta$ and $y = \sum_{i=1}^{N} a_i \sin \theta_i = r \sin \theta$ are derived. The individual amplitudes a_i are random and the phases θ_i have a uniform distribution. According to the central limit theorem, when N is very large, it can be assumed that x and y are both Gaussian variables with means equal to zero and variance:

$$\sigma_x^2 = \sigma_y^2 = \sigma^2. \tag{2-15}$$

Due to x and y are independent random variables, the joint distribution $p(x,y)$ is

$$p(x,y) = p(x)\,p(y) = \frac{1}{2\pi\sigma^2}\exp\left(-\frac{x^2+y^2}{2\sigma^2}\right). \tag{2-16}$$

The distribution $p(r,\theta)$ can be formulated as a function of $p(x,y)$:

$$p(r,\theta) = |J|\,p(x,y), \tag{2-17}$$

where J is defined as

$$J \equiv \begin{vmatrix} \partial x/\partial r & \partial x/\partial\theta \\ \partial y/\partial r & \partial y/\partial\theta \end{vmatrix} = \begin{vmatrix} \cos\theta & -r\sin\theta \\ \sin\theta & r\cos\theta \end{vmatrix} = r. \tag{2-18}$$

Therefore, the distribution can be reformulated as

$$p(r,\theta) = \frac{r}{2\pi\sigma}\exp\left(-\frac{r^2}{2\sigma^2}\right). \tag{2-19}$$

Thus, the Rayleigh fading has a probability distribution function (PDF) :

$$p(r) = \int_0^{2\pi} p(r,\theta)\,d\theta = \begin{cases} \dfrac{r}{\sigma^2}\exp\left(-\dfrac{r^2}{2\sigma^2}\right), & r \geq 0 \\[2mm] 0, & \text{otherwise} \end{cases} \tag{2-20}$$

$$p(\theta) = \frac{1}{2\pi}, \quad \text{-}\pi<\theta<\pi, \tag{2-21}$$

where r is received signal envelope voltage and σ^2 is the average power of the received signal, which can be shown in Figure 2-12. Assume the probability that the envelope of the received signal does not exceed a specified value R is given by the corresponding cumulative distribution function (CDF) :

$$P(R) = p(r \leq R) = \int_0^R p(r)\,dr = 1 - \exp\left(-\frac{R^2}{2\sigma^2}\right) \tag{2-22}$$
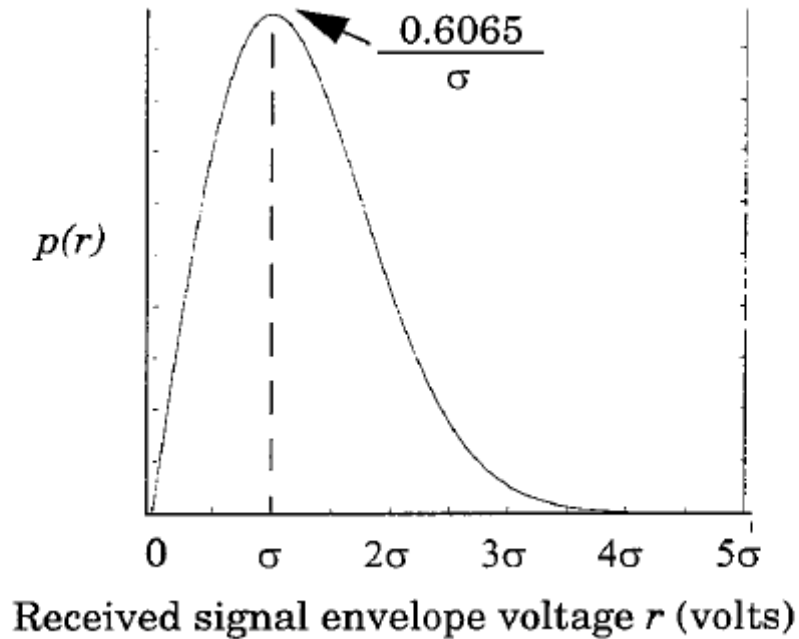
Figure 2-12: Rayleigh PDF

2.4 Wide Sense Stationary Uncorrelated Scattering Channels

Wide sense stationary (WSS) channels have fading statistics that remain constant over short time period. It implies that the correlation functions of channels depend on the time difference $\triangle t$. That can be illustrated that WSS channels give rise to scattering with uncorrelated Doppler shifts.

Uncorrelated scattering (US) channels are described by an uncorrelated attenuation and phase shift with paths of different delays. Bello suggested that US channels are wide sense stationary in the frequency domain so that the correlation functions depend on frequency difference $\triangle f$ [12].

Wide sense stationary uncorrelated scattering (WSSUS) channels are a special

kind of multipath-fading channel. This channel displays uncorrelated scattering in time-delay and Doppler shift. Radio channels are always modeled as WSSUS channels. As regarding WSSUS channels, the correlation functions have singular behavior in time delay and Doppler shift.

2.5 Computer Simulations

For the discussion of the Doppler effect, we use the U-shaped Doppler spectrum defined in Jakes model. The Doppler spectrum in Jakes model is defined as :

$$S(f) = \frac{1.5}{\pi f_m \sqrt{1 - \left(\dfrac{f - f_c}{f_m}\right)^2}}, \quad f \in \left[-f_m, f_m\right]. \tag{2-23}$$

In Figure 2-13, We assume $f_c = 1000$ Hz , $f_m = 50$ Hz , and sampling frequency $f_s = 0.1$ Hz . The Doppler spectrum is U-shaped and symmetrical with f_c . As well as Figure 2-14, we change the Doppler shift such as $f_m = 5$ Hz . It can come to a conclusion that the value of Doppler shift will affect the shape of Doppler power spectrum. In other words, the slow velocity will make the Doppler power spectrum more centralize with f_c .

From the standpoint of fading channel using Jakes model, we assume sampling time $T_s = 1$ ms and number of subpaths $N = 4$. We set the different values of Doppler shift $f_m = 10, \ 50, \text{ and } 100$ Hz in Figure 2-15, Figure 2-16, and Figure 2-17, respectively. Observing these figures, we can come to a conclusion that the coherence time T_C gets smaller as the Doppler shift f_m gets larger. It can justify that the coherence time is inversely proportional to the Doppler shift f_m .

Finally, Figure 2-18 and Figure 2-19 illustrate PDF and CDF of Rayleigh fading by assuming $\sigma = 1$. The peak value of Rayleigh PDF in Figure 2-18 conforms to analytic value $0.6065 / \sigma$.
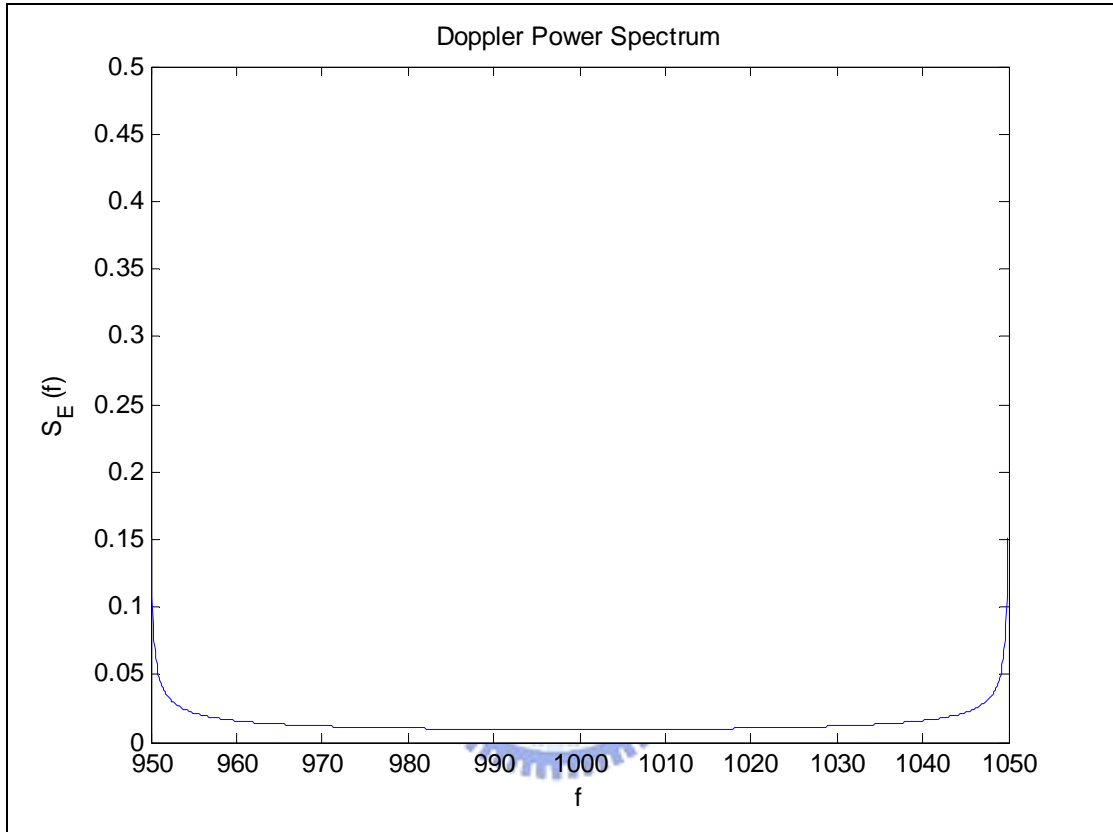
Figure 2-13: Doppler power spectrum with $f_c = 1000$ Hz and $f_m = 50$ Hz
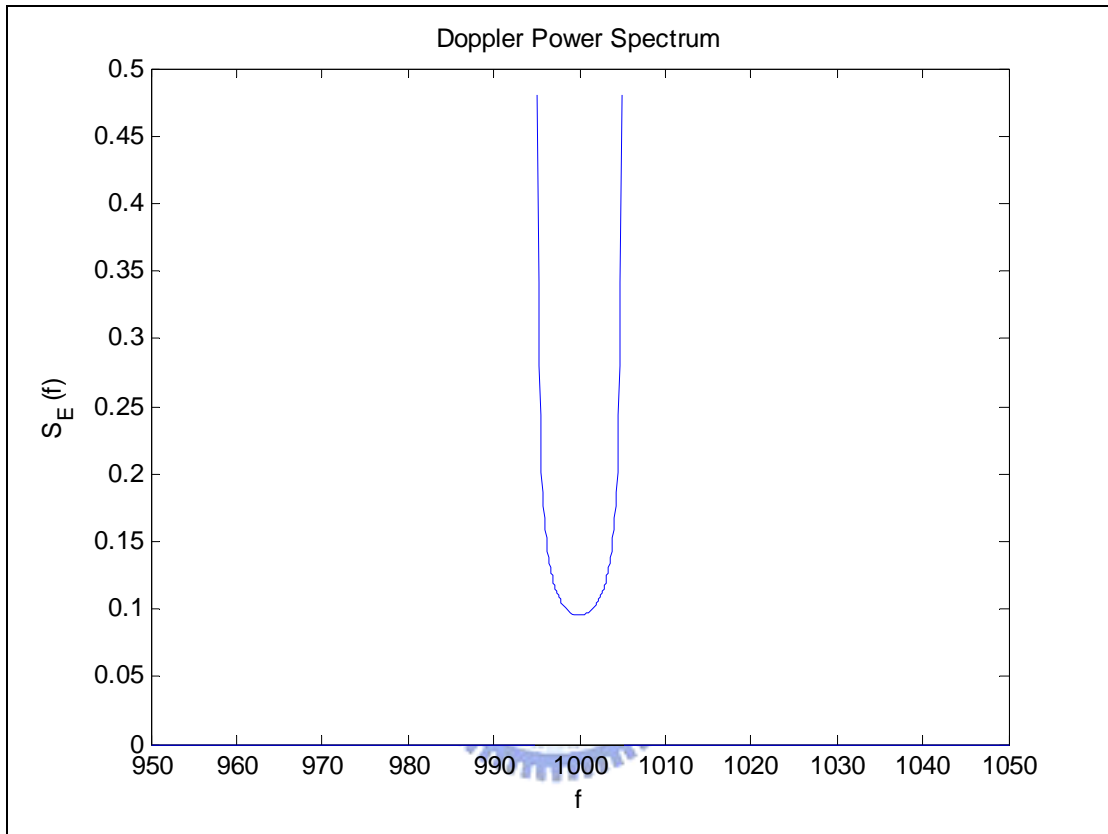
Figure 2-14: Doppler power spectrum with $f_c = 1000$ Hz and $f_m = 5$ Hz
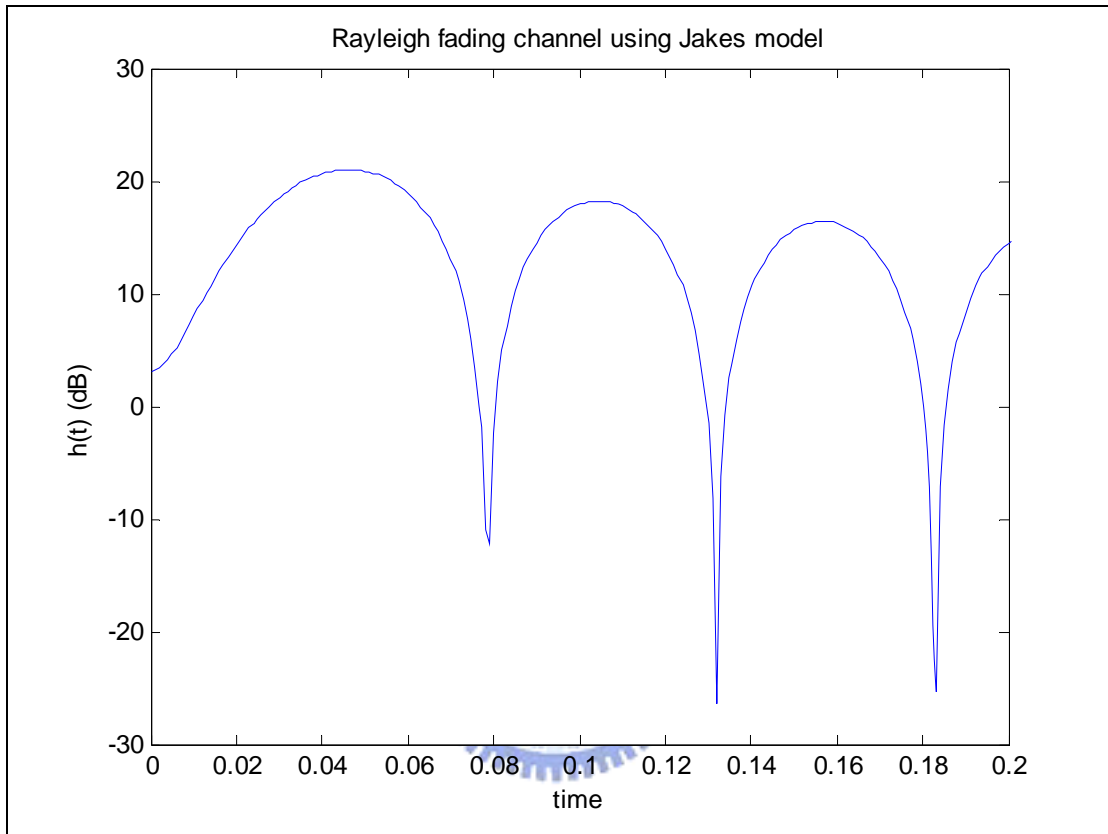
Figure 2-15: Rayleigh fading using Jakes model by setting $f_m = 10$ Hz
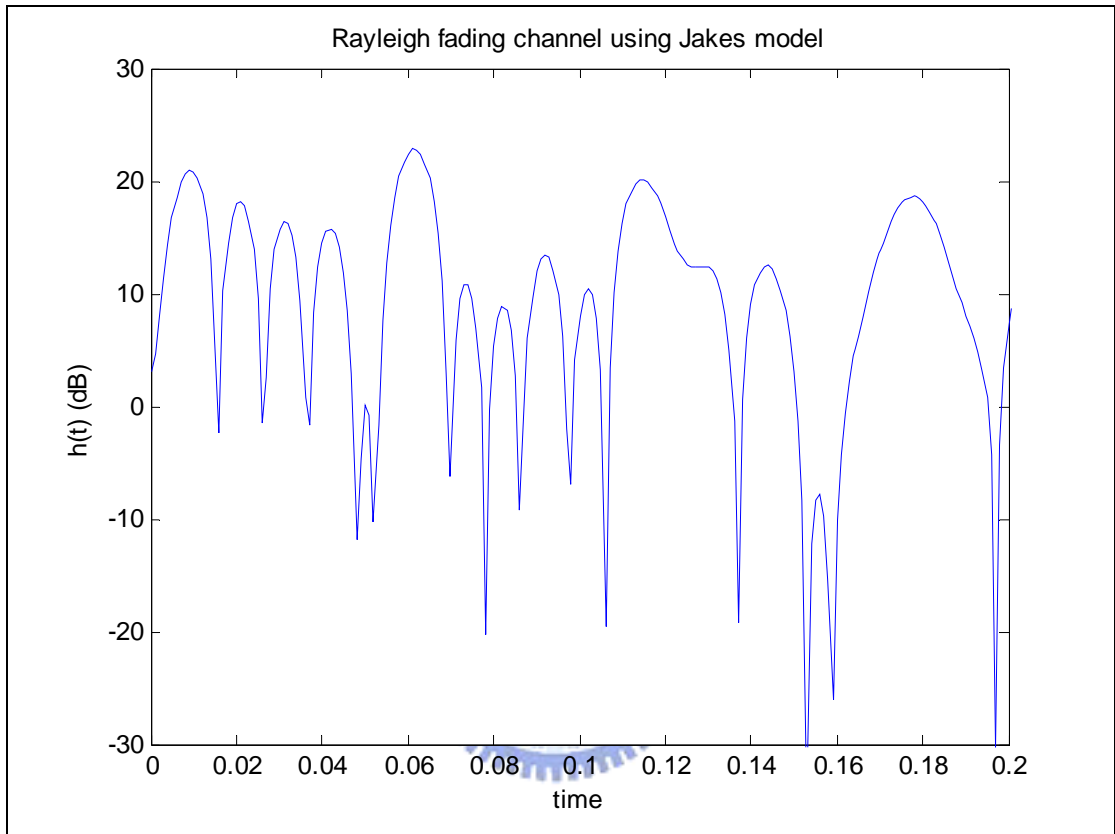
Figure 2-16: Rayleigh fading using Jakes model by setting $f_m = 50$ Hz
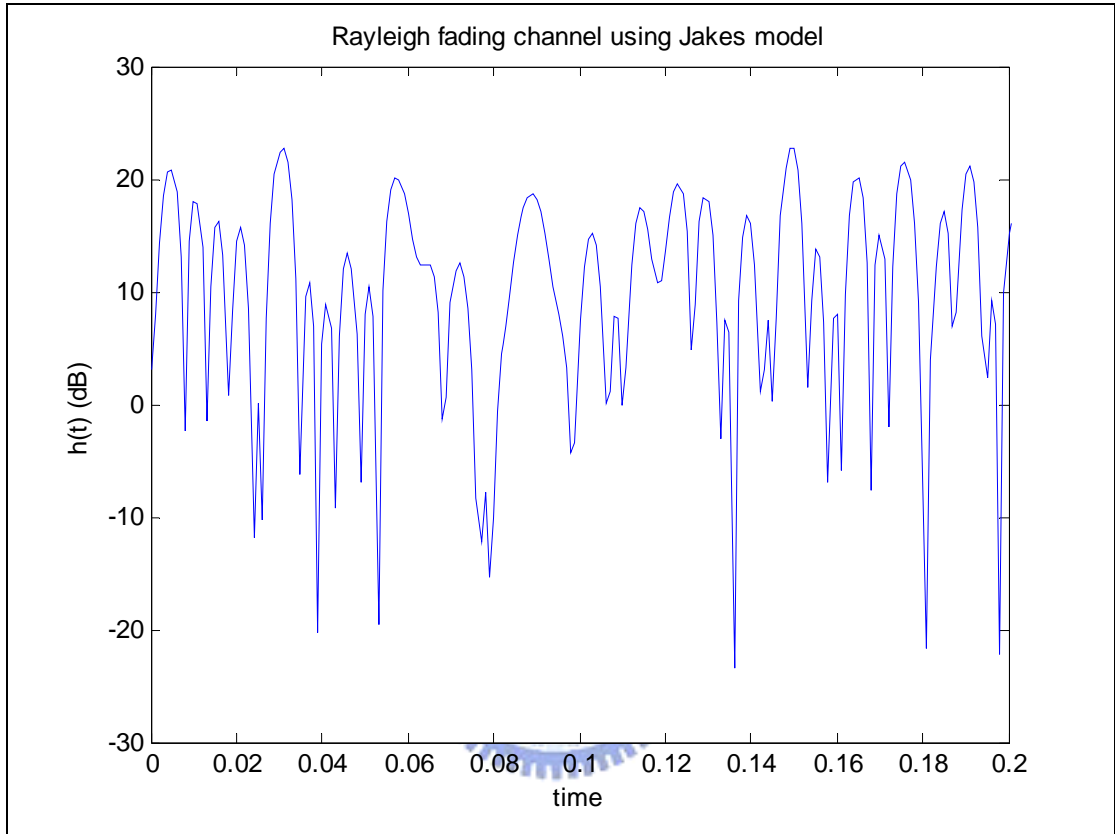
Figure 2-17: Rayleigh fading using Jakes model by setting $f_m = 100$ Hz
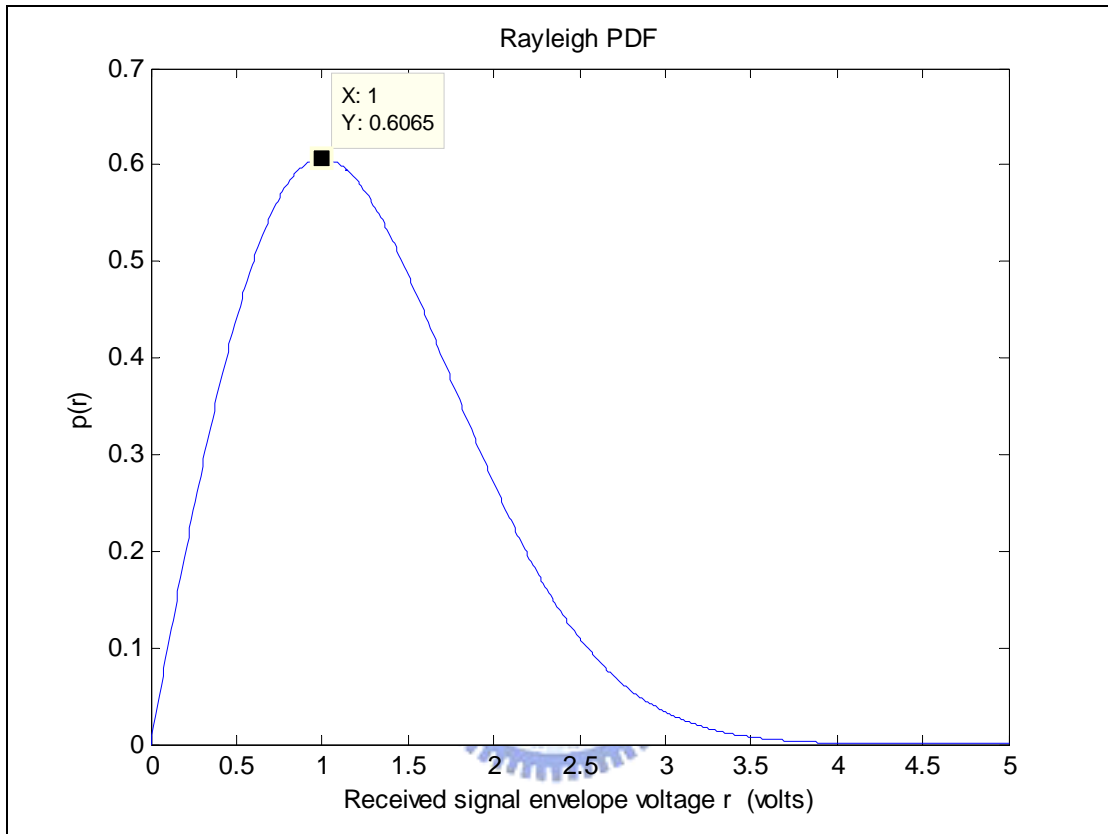
Figure 2-18: Rayleigh probability distribution function for $\sigma = 1$
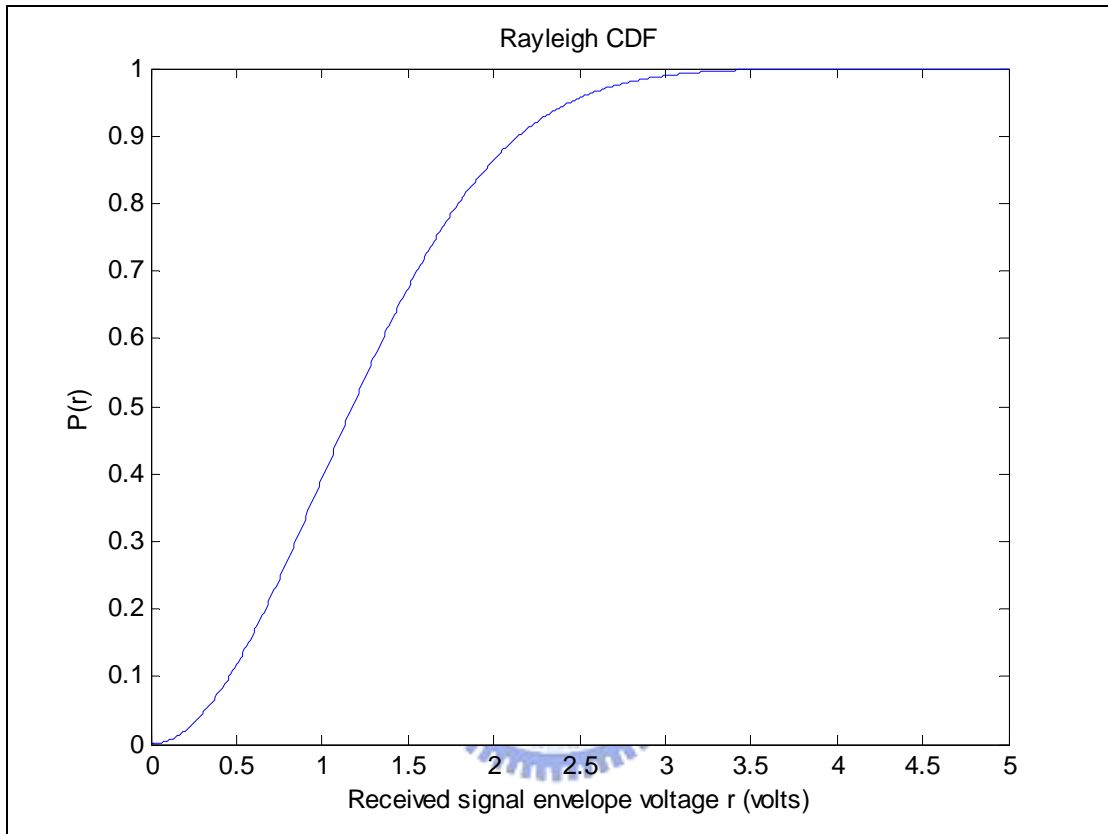
Figure 2-19: Rayleigh cumulative distribution function for $\sigma = 1$

2.6 Summary

In this chapter, the characteristics of the radio propagation and multipath fading phenomenon have been described. For large-scale fading, average received signal power decays logarithmically with T-R separation. This phenomenon is referred to as log-normal shadowing. On the other hand, for small-scale fading, the features can be divided into two kinds of viewpoints : time and frequency. The time and frequency dispersion mechanisms in a radio channel result in four different effects, which are mostly manifested depending on the features of transmitted signal, channel, and velocity. In brief, multipath delay spread causes flat and frequency selective fading and Doppler spread causes slow and fast fading. Both influential factors are independent with the other.

Modeling of multipath fading channels is also described. Rayleigh distribution is followed by multipath fading channels. WSSUS channels are assumed when analyzing the wireless communication systems. Therefore, WSSUS channels are our goal for simulating multipath fading channels. In the following section, we will introduce Jakes model briefly use the Doppler spectrum of Jakes for common.

Chapter 3

Rayleigh Fading Channel Simulators for SISO System

Accurate and fast fading channel simulator is an essential scheme under realistic channel conditions. The new methodologies for efficient simulation of digital communications over Rayleigh fading under the assumption of wide-sense-stationary uncorrelated-scattering (WSSUS) channel are proposed. Common models for simulating fading channel can be divided into three types: direct form, modified Jakes, and Karhunen-Loeve (K-L) expansion models.

In the direct form model, channel is a discrete-time lowpass-equivalent channel impulse response (CIR) with a large number of coefficients. The simplest method for simulating Rayleigh fading is to feed white Gaussian noise (WGN) to a digital filter matched to the respective fading spectrum [13].

For the modified Jakes model, it is widely accepted for the simulation of wireless communication channels. The independent Rayleigh fader uses sum-of-sinusoids for simulations, and its statistical characteristics can approach the desired ones. However in this method, its major disadvantage is high computational complexity and how to provide the multiple uncorrelated fading waveforms. In the K-L expansion model, frequency-selective fading channel is derived from K-L expansion. Under the same mean-square error condition, the number of terms needed by the truncated K-L

expansion is less than that of a series expansion produced by the discrete-path approximation of the channel [14].

The organization of this section is as follows. Section 3.1 describes direct form model. The modified Jakes model and our proposed method using different mathematical forms for random phase are derived in Section 3.2. Section 3.3 develops an efficient K-L expansion model and compares the performance with modified Jakes model. Finally, the method accuracy is demonstrated by computer simulations in Section 3.4 and summary is given in Section 3.5.

3.1 Direct Form Model

Several authors have proposed some methods to modify the accuracy. Komninakis [15] showed that the simulator contains a fixed IIR filter followed by a variable polyphase interpolator, to accommodate different Doppler rates. The IIR filter was designed using an iterative optimization schemes that is more generally applicable and can be used to approximate any given magnitude frequency response. Fenchtel [16] found that a new simulator applied for linear amplitude/phase modulation and linear fading channels including Nyquist filtering .It is shown to be a good approximation to the conventional model in the case of tight rolloff factors

Channel having quasi- or truly continuous delay profiles can now properly illustrated at significantly reduced computational complexity. Furthermore, the new simulator leads to the lowest level of complexity being achieved for the prevailing channel and noise conditions on a particular channel. In this section, we will have more illustrations for the basic idea of direct form method.

Direct form method is a popular kind of Rayleigh fading simulation. In which, using the concept of in-phase and quadrature modulation paths to produce a simulated signal with spectral and temporal characteristics is very close to measured data.

The basic process for simulating Rayleigh fading is shown in Figure 3-1:
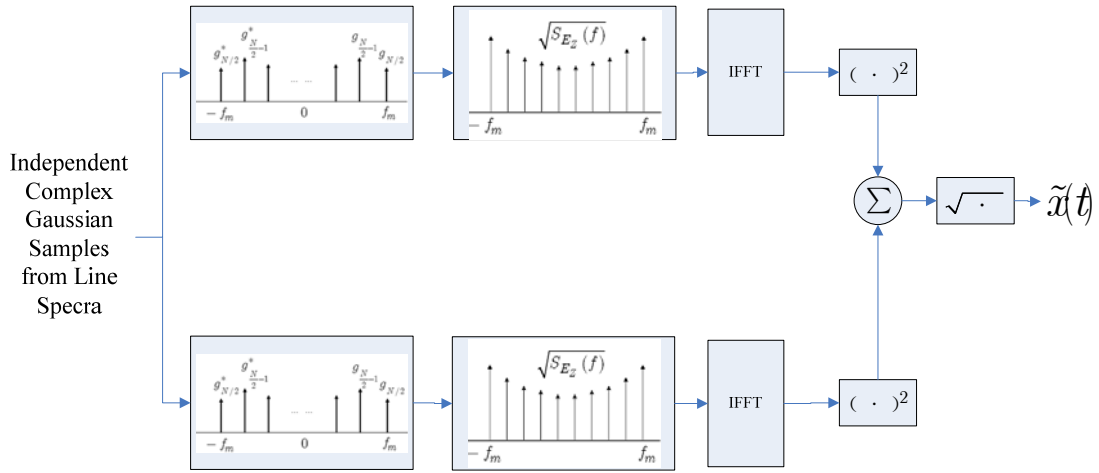
Figure 3-1: Frequency domain implementation of a Rayleigh fading simulator at baseband for narrowband system

To carry out the simulator shown in Figure 3-1, the following steps are used:

Step1: Specifying the number of frequency domain sample points N to represent the maximum Doppler shift f_m, Doppler power spectral density $S_{E_z}(f)$ can be expressed as follows :

$$S_{E_Z}(f) = \frac{1.5}{\pi f_m \sqrt{1 - \left(\frac{f - f_c}{f_m}\right)^2}}$$

(3-1)

where

f_m : the maximum Doppler frequency

f_c : the carrier frequency of the scattered signal

Step2: The frequency spacing is calculated as $\Delta f = 2f_m/(N-1)$ between each spectral lines, where time duration of a fading waveform is $1/\Delta f$.

Step3: Complex Gaussian random variables are generated for each component of $N/2$ positive frequency of the noise source.

Step4: Assigning the conjugating positive frequency values at negative frequency, the negative frequency components are constructed.

Step5: The in-phase and quadratrue noise sources multiply with $\sqrt{S_{E_Z}(f)}$, respectively.

Step6: Operating the inverse fast Fourier transform (IFFT) on the resulting frequency domain signals from the in-phase and quadrature components to get two length N time series, the squares of each signal point in time is added to create an N-point time series.

Step7: Taking the square root of the sum of obtained in Step6, a N-point time series of a simulator of Rayleigh fading signal will be got.

The method mentioned above is used under the condition of flat fading (frequency nonselective fading) in narrowband system. If we want to implement frequency selective fading in wideband system, just need to consider path gain and propagation time delay settings. We will have complete description in Chapter 4.

3.2 Jakes Model and Modified Jakes Models

Rayleigh fading channels are widely using sum-of-sinusoids based on Jakes model method for simulating mobile radio channel. Many different models [19]-[24] focus on approximating the random process by the superposition of a finite number of properly selected sinusoids. Generally, these models can be classified as either statistical or deterministic. The statistical models leave at least one of parameter sets (path amplitudes, random phases, or Doppler frequencies) as time-variant random variables. In contrast, the deterministic models have fixed parameter sets for all simulation trials. The deterministic properties are relatively popular because of their

simplicity.

3.2.1 Clarke Model and Jakes Model

Many approaches have been suggested for modeling Rayleigh fading waveforms. Clarke was the first author to propose the well know mathematical reference model for Rayleigh fading channel [17]. A simplified version of Clarke's model proposed by Jakes has been widely used in three decades [18].

Clarke's reference model defines the complex faded envelope $g(t)$ as:

$$g(t) = g_c(t) + jg_s(t) = \sum_{n=0}^{N-1} C_n e^{j(w_m t \cos \alpha_n + \phi_n)} \tag{3-2}$$

where

N : the number of propagation paths of a single fader

w_m : the maximum Doppler frequency in radius

C_n : the path gain

α_n : the nth angle of arrival which is uniformly distributed on the interval $[-\pi, \pi)$

ϕ_n : the initial phase associated with the nth propagation path which is uniformly distributed on the interval $[-\pi, \pi)$.

By the Central Limit Theorem, the real part $g_c(t) = \mathrm{Re}\{g(t)\}$ and the imaginary part $g_s(t) = \mathrm{Im}\{g(t)\}$ of the complex faded envelope can be approached as Gaussian random process when $N \rightarrow \infty$. Assuming a two dimensional (2-D) isotropic scattering environment, the autocorrelation and cross-correlation function can be described as below:

$$R_{g_c g_c}(\tau) = E[g_c(t) g_c(t+\tau)] = J_0(w_m \tau) \tag{3-3}$$

$$R_{g_s g_s}(\tau) = E\big[g_s(t)\,g_s(t+\tau)\big] = J_0\big(w_m\tau\big) \tag{3-4}$$

$$R_{g_c g_s}(\tau) = R_{g_s g_c}(\tau) = 0 \tag{3-5}$$

$$R_{gg}(\tau) = \frac{1}{2}E\big[g(t)\,g^*(t+\tau)\big] = J_0\big(w_m\tau\big) \tag{3-6}$$

$$R_{|g|^2|g|^2}(\tau) = 4 + 4J_0^2\big(w_m\tau\big), \tag{3-7}$$

where

$E[\cdot]$: the statistical exception operator

$J_0(\cdot)$: the zero-order Bessel function of the first kind.

Without the loss of generality, we can set $\sum\limits_{n=0}^{N} E\big[C_n^2\big] = 1$ and $E_0 = \sqrt{2}$. The probability density function (PDF) of the fading envelope $|g(t)|$ and its phase $\theta_g(t) = \tan^{-1}\left(\dfrac{g_c(t)}{g_c(t)}\right)$ can be given by:

$$f_{|g|}(x) = x\cdot e^{-\frac{x^2}{2}}, \quad x \geq 0 \tag{3-8}$$

$$f_{\theta_g}(\phi) = \frac{1}{2\pi}, \quad \phi \in [-\pi, \pi) \tag{3-9}$$

According to the above equation, the ideal fading envelope $|g(t)|$ is Rayleigh distribution and the phase $\theta_g(t)$ is uniformly distribution.

Jakes Model derived well-known deterministic simulation model for Rayleigh fading channels, based on Clarke's reference model and by selecting $C_n = 1/\sqrt{N}$, $\alpha_n = 2\pi n/N$, and $\phi_n = 0$ for $n = 1, 2, \cdots, N$. The N fading waveforms of a single fader can be reduced to $N_0 = (N-2)/4$. The implementation is shown in Figure 3-2. The normalized low-pass process of this model is given by

$$g(t) = g_c(t) + jg_s(t) \tag{3-10}$$

$$g_c(t) = \frac{2}{\sqrt{N}}\sum_{n=0}^{N_0} a_n \cos\big(w_n t\big) \tag{3-11}$$

$$g_s(t) = \frac{2}{\sqrt{N}} \sum_{n=0}^{N_0} b_n \cos(w_n t) \tag{3-12}$$

where $N = 4N_0 + 2$, and

$$a_n = \begin{cases} \sqrt{2}\cos\beta_0, & n = 0 \\ 2\cos\beta_{n,} & n = 1, 2, \ldots, N_0 \end{cases} \tag{3-13}$$

$$b_n = \begin{cases} \sqrt{2}\sin\beta_0, & n = 0 \\ 2\sin\beta_{n,} & n = 1, 2, \ldots, N_0 \end{cases} \tag{3-14}$$

$$\beta_n = \begin{cases} \dfrac{\pi}{4}, & n = 0 \\ \dfrac{\pi n}{N_0}, & n = 1, 2, \ldots, N_0 \end{cases} \tag{3-15}$$

$$w_n = \begin{cases} w_m, & n = 0 \\ w_m \cos\dfrac{2\pi n}{N}, & n = 1, 2, \ldots, N_0 \end{cases} \tag{3-16}$$
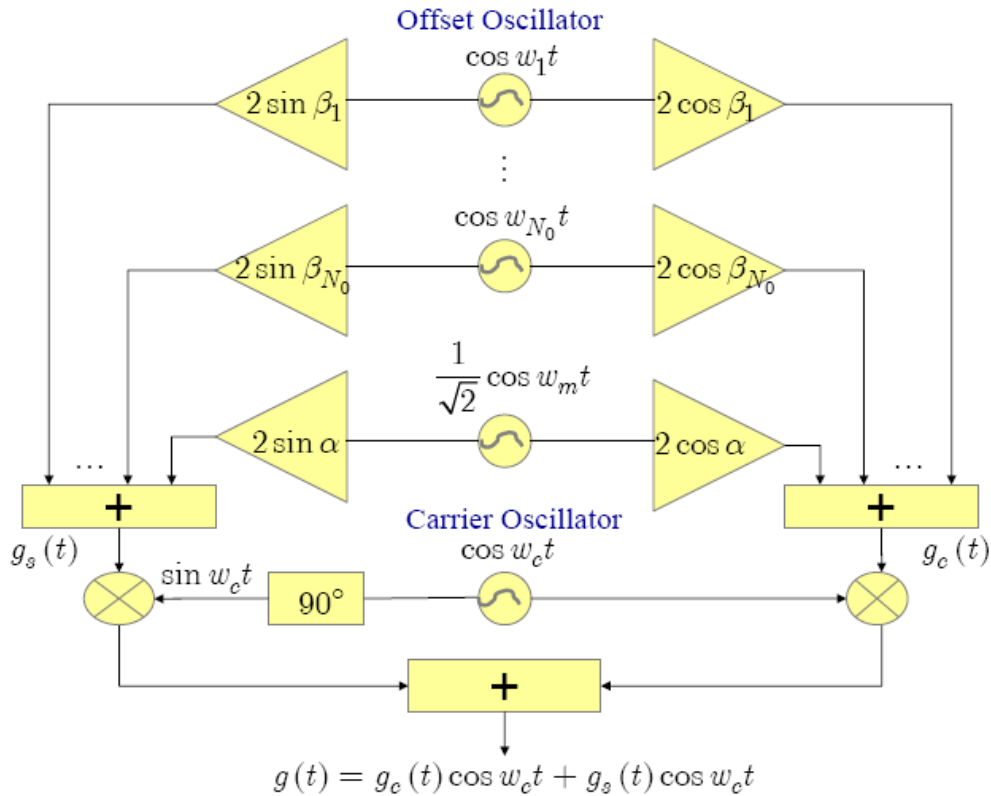
Figure 3-2: Jake fading channel simulator

Jakes simplified simulation of Rayleigh fading channels based on reducing the

number of sinusoids. However, an important shortcoming in the design is that the rays experiencing the same Doppler frequency shift are correlated [19]. This causes the generating signals to be wide-sense-nonstationary. Therefore, various modifications of Jakes Model have been found in the literature.

3.2.2 Development of Modified Jakes Models

Pop and Beaulieu model [20] was suggested by removing the constraint $\phi_n = 0$ of Jakes model and let the phases ϕ_n to be uncorrelated. Assuming there are M independent faders, a single fader will be composed of N waveforms which can be reduced to N_0 as Jakes model. The kth complex faded envelope (fader) can be defined as $g_k(t) = g_{k_c}(t) + jg_{k_s}(t)$, where $k = 0, 1, \ldots, M-1$

$$g_{k_c}(t) = \sqrt{\frac{4}{N}} \cos(\beta_0) \cos(w_m t + \phi_{0k}) + \sqrt{\frac{8}{N}} \sum_{n=1}^{N_0} \cos(\beta_n) \cos(w_m \cos \alpha_n \cdot t + \phi_{nk})$$

(3-17)

$$g_{k_s}(t) = \sqrt{\frac{4}{N}} \sin(\beta_0) \cos(w_m t + \phi_{0k}) + \sqrt{\frac{8}{N}} \sum_{n=1}^{M} \sin(\beta_n) \cos(w_m \cos \alpha_n t + \phi_{nk})$$
,

(3-18)

where

α_n : the nth angle of arrival which is equal to $2\pi n / N$

w_m : the maximum Doppler frequency in radius

β_n : the phase which is equal to $\pi n / N_0$, for $n = 0, 1, \ldots, N_0$

ϕ_{nk} : the initial phase associated with the nth propagation path of the kth

   fader which is uniformly distributed on the interval $[-\pi, \pi)$

Li and Huang model [21] is an ergodic statistical model, which converges to the desired properties in a single simulation trial. The fading model is proposed by

using of asymmetrical arrival angle arrangement and appropriately chosen incident wave phases. The in-phase and quadrature components in any faders are independent, so each fading waveform will be uncorrelated. The number of fading waveforms of a single fader can be reduced to $N_0 = N/4$. The kth complex faded envelope can be defined as $g_k(t) = g_{k_c}(t) + jg_{k_s}(t)$, where $k = 0, 1, \ldots, M-1$

$$g_{k_c}(t) = \sqrt{\frac{1}{N_0}} \sum_{n=0}^{N_0-1} \cos\left(w_m \cos\alpha_{nk} \cdot t + \phi_{nk}^I\right) \qquad (3\text{-}19)$$

$$g_{k_s}(t) = \sqrt{\frac{1}{N_0}} \sum_{n=0}^{N_0-1} \sin\left(w_m \sin\alpha_{nk} \cdot t + \phi_{nk}^Q\right) \qquad (3\text{-}20)$$

where

α_{nk} : the nth angle of arrival in the kth fader which is equal to $\frac{2\pi n}{N} + \frac{2\pi k}{MN} + \alpha_{00}$, where $0 < \alpha_{00} < \frac{2\pi}{MN}$ and $\alpha_{00} \neq \frac{\pi}{MN}$

ϕ_{nk}^I : the initial phase of the inphase component in the kth fader which is uniformly distributed on the interval $[-\pi, \pi)$

ϕ_{nk}^Q : the initial phase of the quadrature component in the kth fader which is uniformly distributed on the interval $[-\pi, \pi)$

Dent model [22] was proposed to modify Jakes model by using orthogonal Walsh-Hadamard codeword to de-correlate the multiple faded envelope. The number of fading waveforms of a single fader can be reduced from N to $N_0 = N/4$. The kth complex faded envelope can be defined as $g_k(t) = g_{k_c}(t) + jg_{k_s}(t)$, where $k = 0, 1, \ldots, M-1$

$$g_{k_c}(t) = \sqrt{\frac{2}{N_0}} \sum_{n=1}^{N_0} A_k(n) \times \left[\cos\left(\beta_n\right) \cdot \cos\left(w_m \cos\alpha_n \cdot t + \phi_n\right)\right] \qquad (3\text{-}21)$$

$$g_{k_s}(t) = \sqrt{\frac{2}{N_0}} \sum_{n=1}^{N_0} A_k(n) \times \left[\sin(\beta_n) \cdot \cos(w_m \cos\alpha_n \cdot t + \phi_n) \right] \qquad (3\text{-}22)$$

where

$A_k(n)$: the kth Walsh-Hadamard code sequence in the nth subpath

(± 1 values)

α_n: the nth angle of arrival which is equal to $2\pi(n - 0.5)/N$

β_n: the phase which is equal to $\pi n / N_0$

ϕ_n: the initial phase associated with the nth propagation path which is

uniformly distributed on the interval $[-\pi, \pi)$

Wu model [23] was proposed for modifying Dent model, the correlation properties are as good as Li and Huang model, which are better than those of Jakes and Dent models. However, the computational complexity of Wu model is just one half of the Li and Huang model. The number of fading waveforms of a single fader can be reduced to $N_0 = N/4$. The kth complex faded envelope can be defined as $g_k(t) = g_{k_c}(t) + jg_{k_s}(t)$, where $k = 0, 1, \ldots, M-1$

$$g_{k_c}(t) = \sqrt{\frac{1}{N_0}} \sum_{n=0}^{N_0-1} A_{k1}(n) \cos(w_m \cos\alpha_{nk} \cdot t + \phi_n) \qquad (3\text{-}23)$$

$$g_{k_s}(t) = \sqrt{\frac{1}{N_0}} \sum_{n=0}^{N_0-1} A_{k2}(n) \cos(w_m \cos\alpha_{nk} \cdot t + \phi_n) \qquad (3\text{-}24)$$

where

$A_{k1}(n)$, $A_{k2}(n)$: the kth orthogonal sequence in n (± 1), which satisfies

$$\frac{1}{N_0} \sum_{n=0}^{N_0-1} A_{kp}^*(n) A_{lq}(n) = \begin{cases} 1, & k = l, \ p = q \\ 0, & \text{else} \end{cases}$$
$$k, l = 0, 1, \ldots, M-1 \quad p, q = 1, 2$$

α_{nk} : the nth angle of arrival in the kth fader which is equal to $\dfrac{2\pi n}{N} + \dfrac{2\pi k}{MN}$

ϕ_n : the initial phase associated with the nth propagation path which is uniformly distributed on the interval $[-\pi, \pi)$

Zheng and Xiao model [24] is not as the same as the above models, it is a typical statistical model. They proposed an improved simulator by introducing random phase shifts in random phase shifts in the low-frequency oscillators to remove the stationary problem from Jakes model. By allowing parameter sets of amplitudes, phases, and Doppler frequencies to be independent random variables, the statistical properties converge to desired values when average over 50 to 100 simulation trials. The number of fading waveforms for simulation can be reduced to $N_0 = N/4$. The kth complex faded envelope can be defined as $g_k(t) = g_{k_c}(t) + jg_{k_s}(t)$, where $k = 0, 1, \ldots, M-1$

$$g_{k_c}(t) = \frac{2}{\sqrt{N_0}} \sum_{n=1}^{N_0} \cos(\psi_{nk}) \cos[w_m \cos \alpha_{nk} \cdot t + \phi_k] \qquad (3\text{-}25)$$

$$g_{k_s}(t) = \frac{2}{\sqrt{N_0}} \sum_{n=1}^{N_0} \sin(\psi_{nk}) \cos[w_m \cos \alpha_{nk} \cdot t + \phi_k] \qquad (3\text{-}26)$$
,

where

α_{nk} : the nth angle of arrival in the kth fader which is equal to

$\dfrac{2\pi n - \pi + \theta_k}{N}$

θ_k : the random of the kth fader phase which is uniformly distributed on the interval $[-\pi, \pi)$

ψ_{nk} : the random phase of the kth fader which is uniformly distributed on the interval $[-\pi, \pi)$

ϕ_k : the initial phase of the kth fader which is uniformly distributed on the

interval $[-\pi, \pi)$

The above models can make a summary as Table 3-1.

Table 3-1: Summary of modern modified Jakes models

	Complex Faded Envelope
Pop and Beaulieu	$g_k(t) = \sqrt{\dfrac{4}{N}} \cos(\beta_0) \cos(w_m t + \phi_{0k}) + \sqrt{\dfrac{8}{N}} \sum_{n=1}^{N_0} \cos(\beta_n) \cos(w_m \cos\alpha_n \cdot t + \phi_{nk})$ $+ j\left\{ \sqrt{\dfrac{4}{N}} \sin(\beta_0) \cos(w_m t + \phi_{0k}) + \sqrt{\dfrac{8}{N}} \sum_{n=1}^{M} \sin(\beta_n) \cos(w_m \cos\alpha_n t + \phi_{nk}) \right\}$
Li and Huang	$g_k(t) = \sqrt{\dfrac{1}{N_0}} \sum_{n=0}^{N_0-1} \cos\left(w_m \cos\alpha_{nk} \cdot t + \phi_{nk}^I\right) + j\sqrt{\dfrac{1}{N_0}} \sum_{n=0}^{N_0-1} \sin\left(w_m \sin\alpha_{nk} \cdot t + \phi_{nk}^Q\right)$
Dent	$g_{k_c}(t) = \sqrt{\dfrac{2}{N_0}} \sum_{n=1}^{N_0} A_k(n) \times \left[\cos(\beta_n) \cdot \cos(w_m \cos\alpha_n \cdot t + \phi_n)\right]$ $+ j\left\{ \sqrt{\dfrac{2}{N_0}} \sum_{n=1}^{N_0} A_k(n) \times \left[\sin(\beta_n) \cdot \cos(w_m \cos\alpha_n \cdot t + \phi_n)\right] \right\}$
Wu	$g_k(t) = \sqrt{\dfrac{1}{N_0}} \sum_{n=0}^{N_0-1} A_{k1}(n) \cos(w_m \cos\alpha_{nk} \cdot t + \phi_n)$ $+ j\sqrt{\dfrac{1}{N_0}} \sum_{n=0}^{N_0-1} A_{k2}(n) \cos(w_m \cos\alpha_{nk} \cdot t + \phi_n)$
Zheng and Xiao	$g_k(t) = \dfrac{2}{\sqrt{N_0}} \sum_{n=1}^{N_0} \cos(\psi_{nk}) \cos\left[w_m \cos\alpha_{nk} \cdot t + \phi_k\right]$ $+ j\dfrac{2}{\sqrt{N_0}} \sum_{n=1}^{N_0} \sin(\psi_{nk}) \cos\left[w_m \cos\alpha_{nk} \cdot t + \phi_k\right]$

3.2.3 Proposed Modified Jakes Model

A novel sum-of-sinusoids Rayleigh fading model is proposed by decomposing the term of initial random phase. In accordance with Clarke's model, we can define the kth complex faded envelope

$$g_k(t) = \sum_{n=0}^{N-1} C_{nk} e^{j(w_m \cos \alpha_{nk} \cdot t + \phi_{nk})} \tag{3-27}$$

where C_{nk}, α_{nk}, w_{nk}, and ϕ_{nk} are the random path gain, the angle of arrival, the angular Doppler frequency, and the initial random phase, respectively. Separating the term of initial random phase, Equation (3-27) will be simplified as

$$g_k(t) = \sum_{n=0}^{N-1} S_{nk} e^{j(w_{nk} \cdot t)} \tag{3-28}$$

where $S_{nk} = C_{nk} e^{j\phi_{nk}}$.

To reduce the number of sinusoid components necessary for the simulation, we can choose $N_0 = N/4$ to be an integer and take into account shifts of the angles α_{nk} and ϕ_{nk} in each quadrant of the circle, then Equation (3-28) can be split into four terms:

$$g_k(t) = \sum_{n=0}^{N_0-1} S_{nk} e^{jw_{nk} \cdot t} + \sum_{n=N_0}^{2N_0-1} S_{nk} e^{jw_{nk} \cdot t} + \sum_{n=2N_0}^{3N_0-1} S_{nk} e^{jw_{nk} \cdot t} + \sum_{n=3N_0}^{4N_0-1} S_{nk} e^{jw_{nk} \cdot t} \tag{3-29}$$

Assuming equal path gain $S_{nk} = S$, and the phase can be reduced like $\phi_{nk} = \phi_{(n+2N_0)k}$, then Equation (3-29) is reformulated as

$$\begin{aligned} g_k(t) &= 2 \sum_{n=0}^{N_0-1} S_{nk} \left(e^{jw_{nk} \cdot t} + e^{jw_{(n+2N_0)k} \cdot t} \right) \\ &\quad + 2 \sum_{n=N_0}^{2N_0-1} S_{nk} \left(e^{jw_{nk} \cdot t} + e^{jw_{(n+2N_0)k} \cdot t} \right) \\ &= 2 \sum_{n=0}^{N_0-1} S_{nk} \left(e^{jw_{nk} \cdot t} + e^{jw_{(n+2N_0)k} \cdot t} \right) \\ &\quad + 2e^{j\frac{\pi}{2}} \sum_{n=0}^{N_0-1} S_{nk} \left(e^{jw_{nk} \cdot t} + e^{jw_{(n+2N_0)k} \cdot t} \right) \end{aligned} \tag{3-30}$$

Therefore, Equation (3-30) can be reformulated as

$$g_k(t) = 2(1+j) \sum_{n=0}^{N_0-1} S_{nk} \left(e^{jw_{nk} \cdot t} + e^{j(w_{nk}+\pi) \cdot t} \right)$$

$$=2(1+j) \sum_{n=0}^{N_0-1} S_{nk} [\cos(w_m \cos\alpha_{nk} \cdot t) + j\sin(w_m \cos\alpha_{nk} \cdot t) \quad \text{(3-31)}$$

$$+ \cos(w_m \cos(\alpha_{nk}+\pi) \cdot t) + j\sin(w_m \cos(\alpha_{nk}+\pi) \cdot t)].$$

We can modify Equation (3-31) by adding Walsh-Hadamard sequences, the Rayleigh fading simulator is defined as

$$g_k(t) = 4 \sum_{n=0}^{N_0-1} S_{nk} (A_{k1}(n) + jA_{k2}(n)) \cos(w_m \cos\alpha_{nk} \cdot t),$$

$$\text{for} \quad k=0,1,...,M-1 \quad \text{(3-32)}$$

where

α_{nk} : the nth angle of arrival in the kth fader which is equal to $\dfrac{2\pi n}{N} + \dfrac{2\pi k}{MN}$

$A_{k1}(n),\ A_{k2}(n)$: the kth orthogonal sequence in n (± 1), which satisfies

$$\frac{1}{N_0} \sum_{n=0}^{N_0-1} A_{kp}^*(n) A_{lq}(n) = \begin{cases} 1, & k=l,\ p=q \\ 0, & \text{else} \end{cases}$$

$$k,l = 0,1,...,M-1 \quad p,q = 1,2$$

S_{nk} : the gain which is equal to $e^{j\beta_{nk}} / \sqrt{N}$

β_{nk} : the random phase which is uniformly distributed on the interval $[-\pi, \pi]$

The statistical properties of new proposed model will be more close to the ones of Clarke reference model than Wu model. It will be shown in Section 3.4. Furthermore, the new model will cost relatively less computational complexity.

3.3 Karhunen-Loeve Expansion Model

This methodology is based on the Karhunen-Loeve (K-L) expansion of time-varying channel output. The K-L expansion requires the minimum number of terms among all possible series expansions in representing a random process for a

given mean-square error. Numerical results have shown that using K-L expansion for simulating fading channel is more efficient. Under the same mean-squared error, the number of terms required by the K-L expansion is less than that required by the discrete-path approximation of the channel in computational complexity.

In the following section, we derive an obvious and understandable method using K-L expansion for Rayleigh fading channel simulation.

3.3.1 Proposed Modified Karhunen-Loeve Expansion Model

The transmitted signal is generally considered to be affected by a random multiplicative fading process with a complex envelope $\tilde{x}(t)$, and its autocorrelation function $R_{\tilde{x}\tilde{x}}(\tau) = J_0\left(w_m\tau\right)$ for $t \in \left[-T/2,\ T/2\right]$. Visintin [25] suggested a convenient approximation of the Bessel function to express the fading process. We adopt Visintin's approximation of Bessel function, then propose a close form and derive a novel of fading simulation by using K-L expansion. The overall procedure can be shown in Figure 3-3.

First, expanding the random process of a single Rayleigh fader $x(t)$ by the K-L expansion is given by

$$x(t) = \lim_{N \to \infty} \tilde{x}(t), \quad -\frac{T}{2} \le t \le \frac{T}{2}, \tag{3-33}$$

where

$$\tilde{x}(t) = \sum_{k=1}^{2N+2} A_k \varphi_k(t) \tag{3-34}$$

The coefficients A_k are independent complex Gaussian random variables of variance λ_k, and $\varphi_k(t)$ are the complex eigenfunctions of $J_0(\cdot)$ which satisfy the following equation:

$$\int_{-\frac{T}{2}}^{\frac{T}{2}} J_0\left[w_m\left(t - \tau\right)\right]\varphi_k\left(\tau\right)d\tau = \lambda_k\varphi_k\left(t\right) \tag{3-35}$$

with $\lambda_1 \geq \lambda_2 \geq \lambda_3 \ldots$, while satisfying the orthonormality constraints

$$\left\langle \varphi_i\left(t\right), \; \varphi_i\left(t\right)\right\rangle = \int_{-\frac{T}{2}}^{\frac{T}{2}} \varphi_i\left(t\right)\varphi_j\left(t\right)dt = \delta\left(i - j\right), \tag{3-36}$$

where $\delta\left(\cdot\right)$ is Kronecker delta function.

However, the integral Equation (3-35) can not be solved straightforward. We can solve Equation (3-35) by using approximation of Bessel function proposed by Jakes. The following steps will derive the complex eigenfunctions and variance.

Step1 : We adopt the idea of [25] for using the Bessel function approximation which can transfer the autocorrelation from continuous to discrete.

$$J_0\left(w_m\tau\right) \simeq \frac{1}{2N+1}\left\{\cos\left(w_m\tau\right) + 2\sum_{n=1}^{N}\cos\left[w_m\tau\cos\left(\frac{\pi n}{2N+1}\right)\right]\right\}$$

$$= \frac{1}{2N+1}\left\{\sum_{n=\pm 1}\frac{e^{jh(n)w_m\tau}}{2} + \sum_{\substack{n=-N \\ (n\neq 0)}}^{N} e^{jg(n)w_m\tau}\right\}, \tag{3-37}$$

where

$$h\left(n\right) = \begin{cases} 1, & \text{if n}>0 \\ -1, & \text{if n}<0 \end{cases} \quad \text{and} \quad g\left(n\right) = h\left(n\right)\cos\left[\frac{n\pi}{2N+1}\right].$$

The above approximation givens an error $< 10^{-3}$ for $x \leq 1.7$ with $N = 1$, for $x \leq 5$ with $N = 2$, etc. Therefore, the choice of index N will be concerned with the error in the evaluation of $J_0\left(w_m\tau\right)$ satisfies the desired precision.

Step2 : Solving the integral Equation (3-35) with Bessel function approximation is derived from Step1, for $\beta \in \left[-A, \; A\right]$

49

$$\int_{-A}^{A} J_0(\alpha - \beta)\theta(\beta)d\beta$$

$$= \sum_{n=\pm 1} \frac{1}{2(2N+1)} e^{jh(n)\alpha} \cdot \left[\int_{-A}^{A} e^{-jh(n)\beta}\theta(\beta)d\beta\right]$$

$$+ \sum_{\substack{n=-N \\ (n\neq 0)}}^{N} \frac{1}{(2N+1)} e^{jg(n)\alpha} \cdot \left[\int_{-A}^{A} e^{-jh(n)\beta}\theta(\beta)d\beta\right] \qquad (3\text{-}38)$$

$$= \sum_{n=\pm 1} Y(n)e^{jh(n)\alpha} + \sum_{\substack{n=-N \\ (n\neq 0)}}^{N} W(n)e^{jg(n)\alpha}$$

where $\alpha = w_m t$, $\beta = w_m \tau$, $\theta(\beta) = \varphi(\beta/w_m)$, and $A = w_m T/2$

$$Y(n) = \frac{1}{2(2N+1)}\int_{-A}^{A} e^{-jh(n)\beta}\theta(\beta)d\beta \qquad (3\text{-}39)$$

$$W(n) = \frac{1}{(2N+1)}\int_{-A}^{A} e^{-jg(n)\beta}\theta(\beta)d\beta. \qquad (3\text{-}40)$$

Step 3 : Equation (3-38) can be reformulated as

$$\sum_{n=\pm 1} Y(n)e^{jh(n)\alpha} + \sum_{\substack{n=-N \\ (n\neq 0)}}^{N} W(n)e^{jg(n)\alpha} = \mu\theta(\alpha) \qquad (3\text{-}41)$$

Step 4 : The coefficients $V(n)$ and $Z(n)$ can be determined by substituting Equation (3-41) into (3-39) and (3-40).

$$\mu Y(n) = \frac{1}{2(2N+1)}\left\{\sum_{m=\pm 1} Y(m)\int_{-A}^{A} e^{j(h(m)-h(n))\beta}d\beta + \sum_{\substack{m=-N \\ (m\neq 0)}}^{N} W(m)\int_{-A}^{A} e^{j(g(m)-h(n))\beta}d\beta\right\}$$

$$= \frac{1}{2(2N+1)}\left\{\sum_{m=\pm 1} Y(m)\frac{e^{j(h(m)-h(n))A} - e^{-j(h(m)-h(n))A}}{j(h(m)-h(n))}\right.$$

$$\left. + \sum_{\substack{m=-N \\ (m\neq 0)}}^{N} W(m)\frac{e^{j(g(m)-h(n))A} - e^{-j(g(m)-h(n))A}}{j(g(m)-h(n))}\right\}$$

$$= \frac{1}{(2N+1)}\left\{\sum_{m=\pm 1} Y(m)\sin c\big[A(h(m)-h(n))\big] + \sum_{\substack{m=-N \\ (m\neq 0)}}^{N} W(m)\sin c\big[A(g(m)-h(n))\big]\right\}$$

for $k = \pm 1$

$$(3\text{-}42)$$

$$\mu W\left(n\right)=\frac{1}{2\left(2N+1\right)}\left\{\sum_{m=\pm 1}Y\left(m\right)\int_{-A}^{A}e^{j\left(h\left(m\right)-g\left(n\right)\right)\beta}d\beta+\sum_{\substack{m=-N \\ (m\neq 0)}}^{N}W\left(m\right)\int_{-A}^{A}e^{j\left(g\left(m\right)-g\left(n\right)\right)\beta}d\beta\right\}$$

$$=\frac{1}{2\left(2N+1\right)}\left\{\sum_{m=\pm 1}Y\left(m\right)\frac{e^{j\left(h\left(m\right)-g\left(n\right)\right)A}-e^{-j\left(h\left(m\right)-g\left(n\right)\right)A}}{j\left(h\left(m\right)-g\left(n\right)\right)}\right.$$

$$\left.+\sum_{\substack{m=-N \\ (m\neq 0)}}^{N}W\left(m\right)\frac{e^{j\left(g\left(m\right)-g\left(n\right)\right)A}-e^{-j\left(g\left(m\right)-g\left(n\right)\right)A}}{j\left(g\left(m\right)-g\left(n\right)\right)}\right\}$$

$$=\frac{1}{\left(2N+1\right)}\left\{\sum_{m=\pm 1}Y\left(m\right)\sin c\left[A\left(h\left(m\right)-g\left(n\right)\right)\right]+\sum_{\substack{m=-N \\ (m\neq 0)}}^{N}W\left(m\right)\sin c\left[A\left(g\left(m\right)-g\left(n\right)\right)\right]\right\}$$

for $k=-N,...,N, \quad k\neq 0$

(3-43)

Step 5 : Reformulate Equation (3-42) and (3-43) as matrix

$$\mathbf{HV}=\mu\mathbf{V} \tag{3-44}$$

where the eignevalues are $\mu=diag\left[\lambda_1\ \lambda_2\ \cdots\ \lambda_{(2N+2)}\right]$, the coefficients can

be represented as

$$\mathbf{V}=\left[Y\left(1\right)\ Y\left(-1\right)\ W\left(N\right)\ \cdots\ W\left(1\right)\ W\left(-1\right)\ \cdots\ W\left(-N\right)\right]$$

and the H matrix with dimensions $\left(2N+2\right)\times\left(2N+2\right)$ can be formulated as

$$\mathbf{H}=\begin{bmatrix}\mathbf{H_{11}} & \mathbf{H_{12}} \\ \mathbf{H_{21}} & \mathbf{H_{22}}\end{bmatrix}$$

$$\mathbf{H_{11}}\left(i,j\right)=\sin c\left\{A\left[h\left((-1)^{j-1}\right)-h\left((-1)^{i-1}\right)\right]\right\},\quad i=1,2\quad j=1,2$$

$$\mathbf{H_{12}}\left(i,j\right)=\sin c\left\{A\left[g\left(\rho\left(j-2\right)\right)-h\left((-1)^{i-1}\right)\right]\right\},\quad i=1,2\quad j=3,4,...,(2N+2)$$

$$\mathbf{H_{21}}\left(i,j\right)=\sin c\left\{A\left[h\left((-1)^{i-1}\right)-g\left(\rho\left(j-2\right)\right)\right]\right\},\quad i=3,4,...,(2N+2)\quad j=1,2$$

$$\mathbf{H_{21}}\left(i,j\right)=\sin c\left\{A\left[g\left(\rho\left(i-2\right)\right)-g\left(\rho\left(j-2\right)\right)\right]\right\},\quad i=3,4,...,(2N+2)\quad j=3,4,...,(2N+2)$$

and $\rho=\left[N,N-1,...,1,-1,...,-(N-1),-N\right]$

Step 6 : The coefficients of **V** are be derived at above step, and the orthonormal basis

$\varphi(t) = \theta(w_m t)$ will be gotten.

Step 7 : If the bases are not orthogonal with each other, we can do Gram-Schmidt

procedure to get new basis. Assume $\varphi_i(t)$ is not orthogonal to $\varphi_j(t)$, with

$i > j$, the new basis $\varphi'_j(t)$ will be

$$\varphi'_j(t) = \varphi_i(t) - \langle \varphi_i(t), \varphi_j(t) \rangle \varphi_j(t). \tag{3-45}$$

The new bases will be all orthogonal among themselves.

K-L expansion models for fading process will be efficient than modified Jakes models. In regard to accuracy, we can observe the statistical properties of K-L expansion models relatively approach the desired ones. As far as computational efficiency concerned, K-L expansion model costs more set-up time. However, K-L expansion model will save more run-time. The advantage of K-L expansion models will be proven in the Section 3.4.
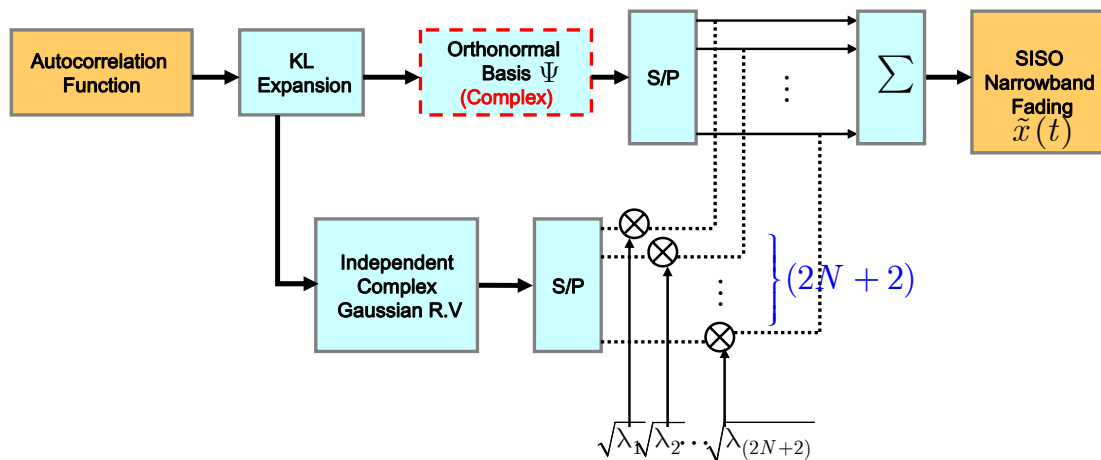

Figure 3-3: K-L expansion for simulating fading channel

3.3.2 Computation Reduction by Using Chebyshev Approximation

We propose a method by using Chebyshev polynomials to save more run-up time for computational loading. The orthonormal bases of K-L expansion models can be approached as Chebyshev Polynomials. The $(l+1)$th degree Chebyshev polynomial of the first kind $T_{l+1}(t)$ is defined as

$$
\begin{aligned}
T_0(t) &= 1 \\
T_1(t) &= t \\
&\vdots \\
T_{l+1}(t) &= 2tT_l(t) - T_{l-1}(t)
\end{aligned}
\tag{3-46}
$$

Chebyshev polynomials are a sequence of orthogonal polynomials and easy to implement because of the recurrence relation. Each degree Chebyshev polynomial is mutually orthogonal, it can be observed obviously in Figure 3-4. Because of the the properties of orthogonality and recursion K-L expansion basis can be replaced with Chebyshev polynomial for reducing computational complexity.

For applying Chebyshev polynomial, the procedure is derived as follows. First, the orthonormal $2N+2$ bases obtained from K-L expansion models are approximated as polynomials by curvefitting. The kth basis polynomial with degree P is described as

$$
\varphi_k(t) = \phi_{kP}(t)t^{(P-1)} + \phi_{k(P-1)}(t)t^{(P-2)} + \cdots + \phi_{k1}(t), \quad \text{for } k = 1,2,\ldots,2N+2.
\tag{3-47}
$$

We can truncate the bases to be a matrix Ψ, and it is equal to the weighting matrix $\mathbf{W}$ multiply with the Chebyshev polynomials truncated matrix $\mathbf{R}$ as Figure 3-5. It can be derived as a linear equation:

$$
\Psi = \mathbf{W}\mathbf{R},
\tag{3-48}
$$

with the $\Psi = \begin{bmatrix} \varphi_1(t) & \varphi_2(t) & \cdots & \varphi_{2N+2}(t) \end{bmatrix}^T$ having dimensions $(2N+2) \times P$, the $\mathbf{W}$ having dimensions $(2N+2) \times L$, and the $\mathbf{R} = \begin{bmatrix} T_1(t) & T_2(t) & \cdots & T_L(t) \end{bmatrix}^T$ having dimensions $L \times P$. The element $T_l(t)$ is the first lth degree Chebyshev polynomial of the first kind.

The choice of degree L will affect the precision of Chebyshev approximation. Higher degree will have more accuracy in fitting basis, and vice versa. However, excess degree increases the computational complexity. The tradeoff will be illustrated in the Section 3.4.
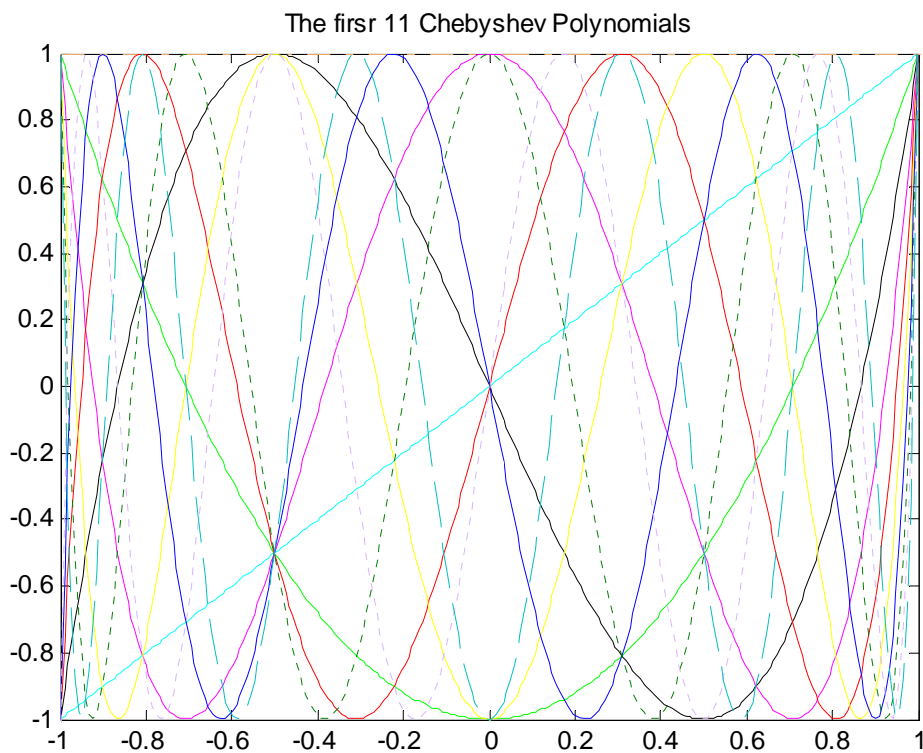

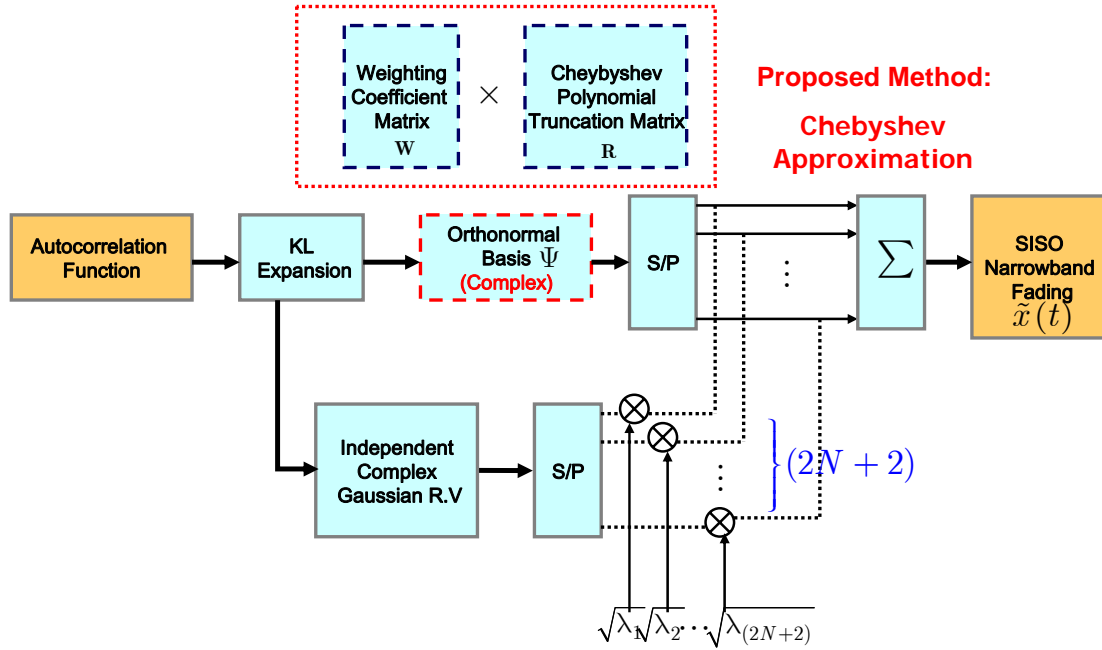**Figure 3-4:** The first 11 degree polynomials

Figure 3-5: K-L expansion basis substituting with Chebyshev polynomial

3.4 Computer Simulations

3.4.1 Comparisons of Modern Modified Jakes Model

This section compares the performance of existing modified Jakes model mentioned in Section 3.2. In all simulations, we set carrier frequency $f_c = 900 \text{ MHz}$, MS mobility speed $v = 100 \text{ km/hr}$, and the maximum Doppler frequency will be $f_m = vf_c / C$ (C is the speed of light about $3 \times 10^8 \text{ m/s}$). Using the symbol rate $S = 64 \text{ kbps}$, we can calculate the sampling period $T_S = 1/S$. For all models, we assume $N = 128$ and $M = 2$.

Figure 3-6 shows the comparison of normalized autocorrelation function of the 1-st fader. The theoretical value is equal to $J_0(w_m\tau)$. Li and Huang model can mostly approximate the desired statistical value. However, it will cost the most plenty computational complexity than other models. Although the autocorrelation property of Wu model is not as good as that of other models, the computational complexity of Wu

model is only half of Li and Huang model.

Figure 3-7 shows the comparison of normalized cross-correlation function between 1-st and 2-nd fader. In order to have the uncorrelated scatters, the theoretical value of cross-correlation is equal to 0. Similar to autocorrelation property, Li and Huang model has the lowest cross-correlation. However, the cross-correlation of Wu model is virtually low as Li and Huang model.
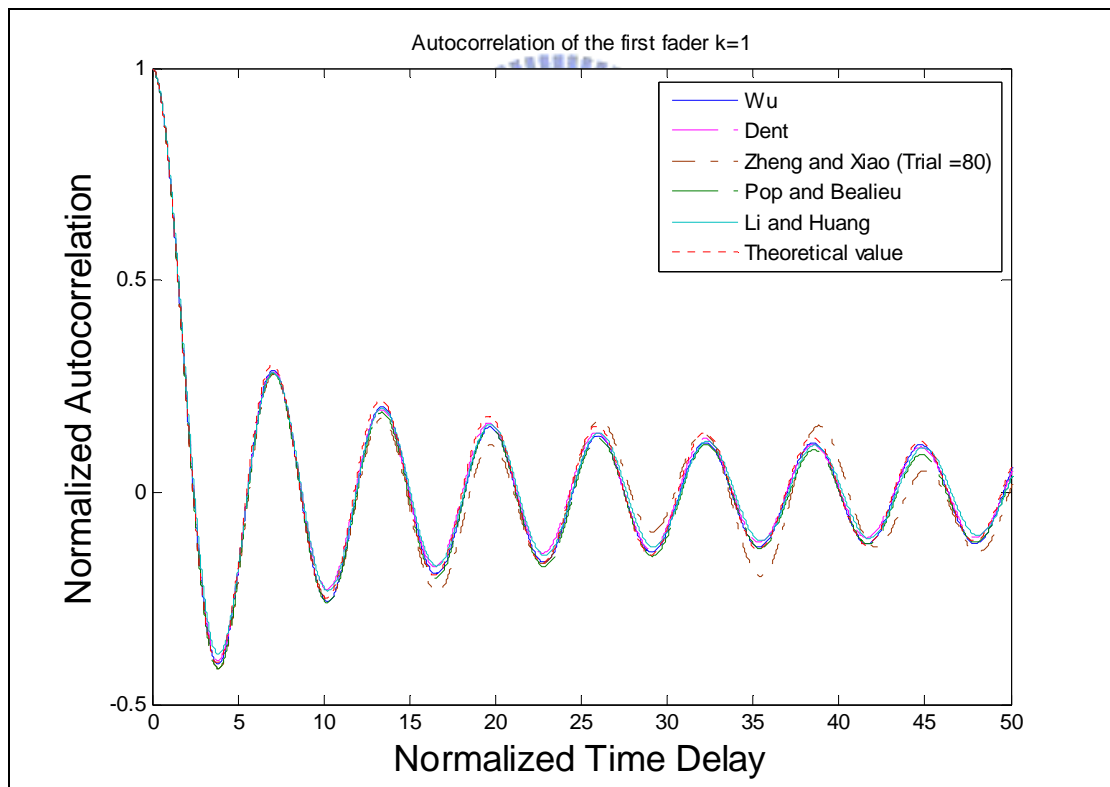

Figure 3-6 : Autocorrelation functions of the 1st fader of the existing modified Jakes models ($N = 128, M = 2$)
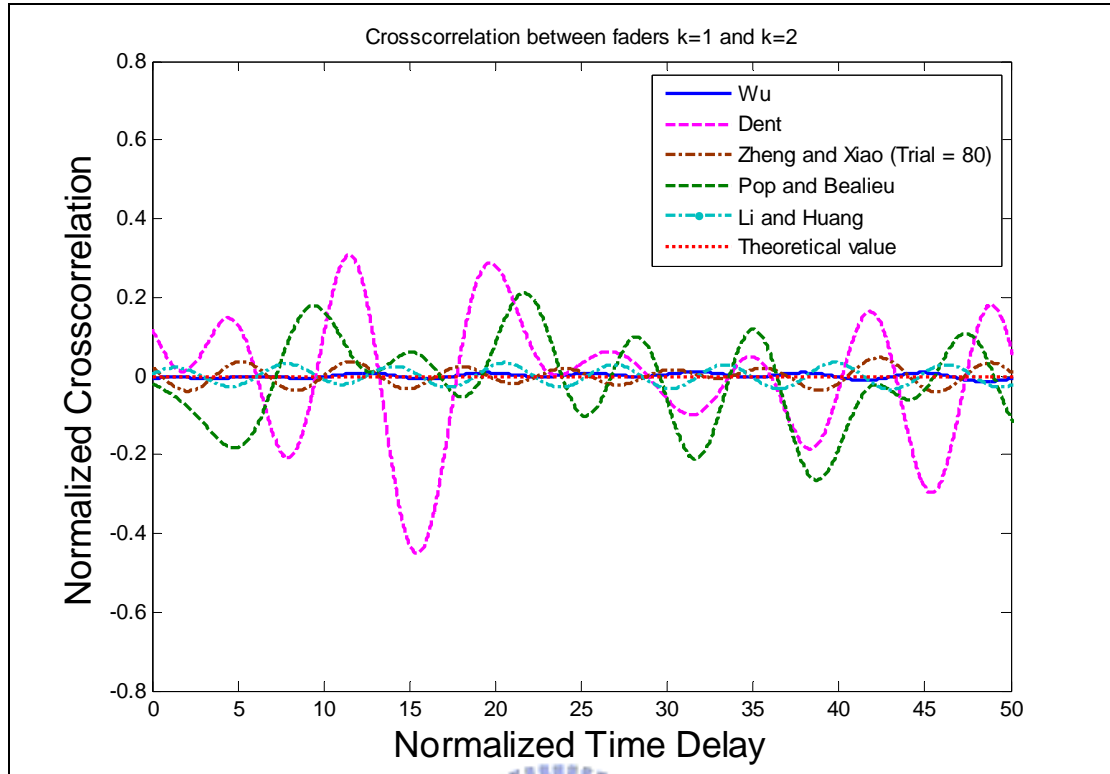
Figure 3-7: Cross-correlation functions of the 1st fader and 2nd fader of the existing modified Jakes models ($N = 128, M = 2$)

3.4.2 Comparisons of Wu Model and Proposed Modified Jakes Model

We choose Wu model to compare with the proposed modified Jakes model. Because our motivation is in want of the efficiency for fading simulator. The proposed modified Jakes model adds the Walsh-Hadamard code which is also applied in Wu model. Comparing to Wu model, the proposed modified Jakes model can slightly have more accuracy under requiring almost computational complexity.

Figure 3-8 shows the autocorrelation comparison between Wu model and proposed modified Jakes model. We can see the proposed model can be slightly more close to the desired statistical value $J_0(w_m\tau)$ than Wu model. The property can reform the disadvantage of Wu model and save more computation time.

Figure 3-9 shows the cross-correlation comparison of Wu model and the proposed modified Jakes model. The proposed modified Jakes model is almost uncorrelated according to the cross-correlation function. The un-correlation between faders of the proposed modified Jakes model is better than that of Wu model.

The advantage of statistical properties of the proposed modified Jakes model may be exhibited by the mean square error (MSE). The MSE is defined as

$$\frac{1}{N} \sum_{i=1}^{N} (g_i - \eta_i)_{,}$$
(3-49)

where the sampling signal g_i and the sampling theoretical signal η_i both have N sampling points. The MSE of autocorrelation and cross-correlation is listed in Table 3-2. Therefore, from the standpoint of computational complexity and statistical accuracy, we can suggest the proposed modified Jakes model has better performance.
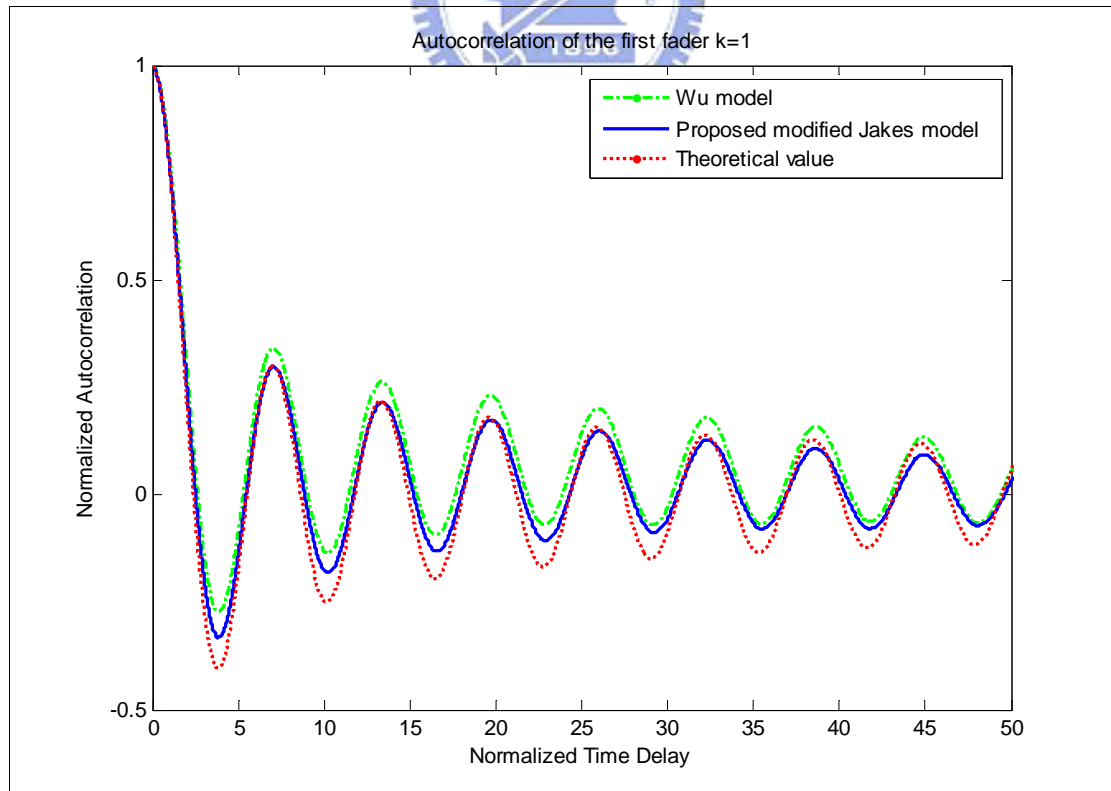
Figure 3-8: Autocorrelation functions of the 1st fader of Wu model and proposed modified Jakes model ($N = 128$, $M = 2$)
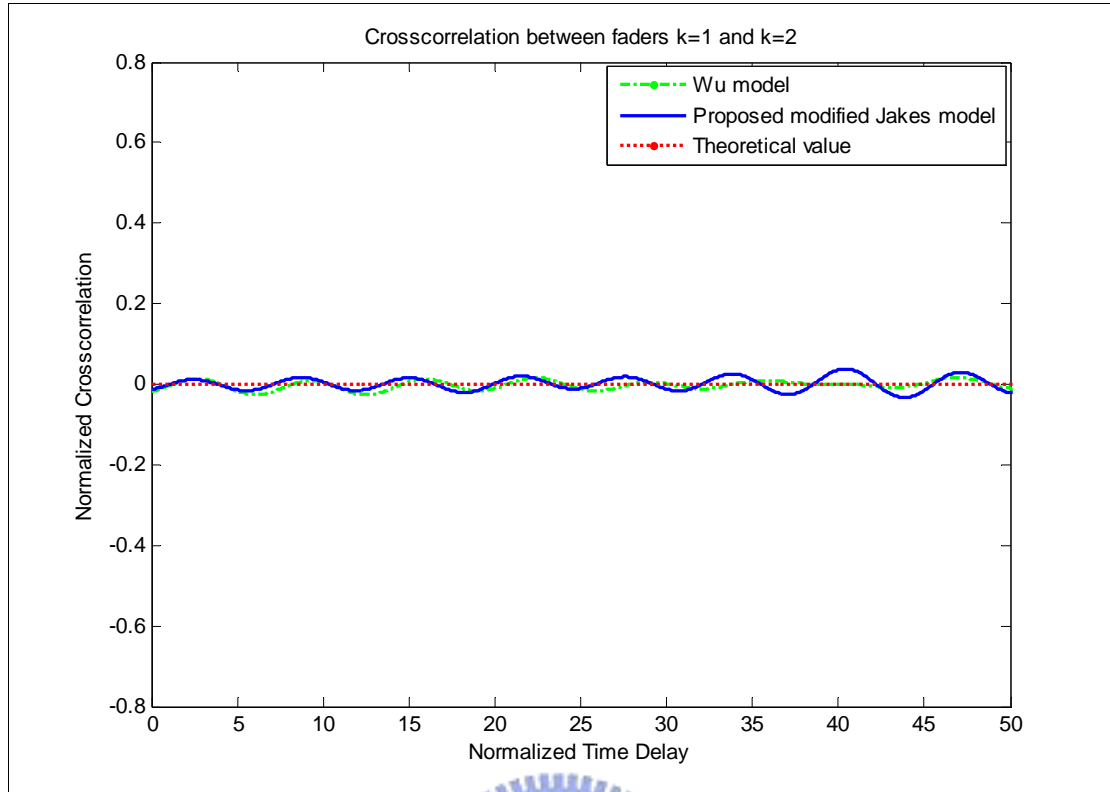
Figure 3-9: Cross-correlation functions of the 1st fader and 2nd fader of Wu model and proposed modified Jakes model ($N = 128, M = 2$)

Table 3-2: Mean-square-error of 1st fader autocorrelation functions and 1st & 2nd faders cross-correlation functions

	Wu Model	**Proposed modified Jakes model**
Autocorrelation	4.7×10^{-3}	1.5×10^{-3}
Cross-correlation	4.0×10^{-5}	1.6×10^{-7}

3.4.3 Comparisons of Modified K-L Expansion Model and Proposed Modified Jakes Model

In this section, we demonstrate the model using the concept of K-L expansion method will be better than the proposed modified Jakes model. First, we set the parameters: $A = 8.1812$ and $N = 2$ for the proposed modified K-L expansion

model. The parameters in the proposed modified Jakes model are $N = 128$ and $M = 2$. Assuming the sampling period $T_S = w_m / S$, w_m and S are the same as above simulation. In Comparison with Jakes model, the Rayleigh fading simulator using the concept of K-L expansion method will cost more setting-time, but it will have quite less run-time in simulation. The proposed modified K-L expansion model saves much time by means of determining eigenfunctions firstly. In reality, we only care about the cost of run-time in the simulation.

Figure 3-10 reveals the comparison of autocorrelation function by different methods in simulating Rayleigh fading channels. Autocorrelation function of proposed modified K-L expansion model is relatively accurate than that of proposed modified Jakes model. Because K-L expansion method is to get signal by decomposing its autocorrelation function, the signal will be more close to the statistical characteristics. The accurate normalized time range is relative to the choice of basis number, so the accuracy of the statistical property using K-L expansion model is effective in $w_m \tau < 5$ for $N = 2$.

In comparison with the cross-correlation of proposed modified Jakes model, Figure 3-11 displays the faders of the proposed modified K-L expansion model are more uncorrelated. Rayleigh faders are uncorrelated with each other while using K-L expansion model for simulating. The cross-correlation between faders will be mainly affected by the independence of generating complex Gaussian random variables. If the variables are mutually independent, the cross-correlation between faders will be diminished.

Observing the simulation result, we can say that the proposed Rayleigh fading simulator using K-L expansion model is more efficient. There are some researches which can solve the problem of dependence of the procedure for generating random variables [26]. Hence, fast and accurate Rayleigh fading simulator can be achieved by

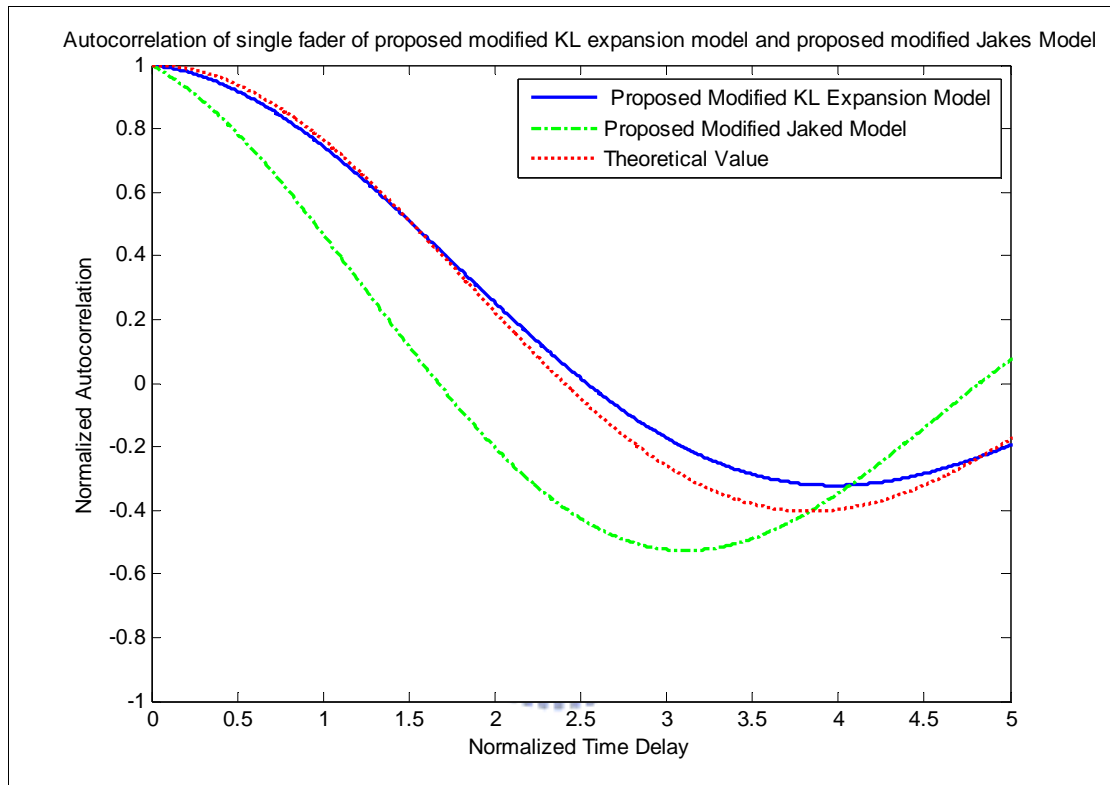our proposed modified K-L expansion model.

Figure 3-10: Autocorrelation functions of proposed modified Jakes model and proposed modified K-L expansion model
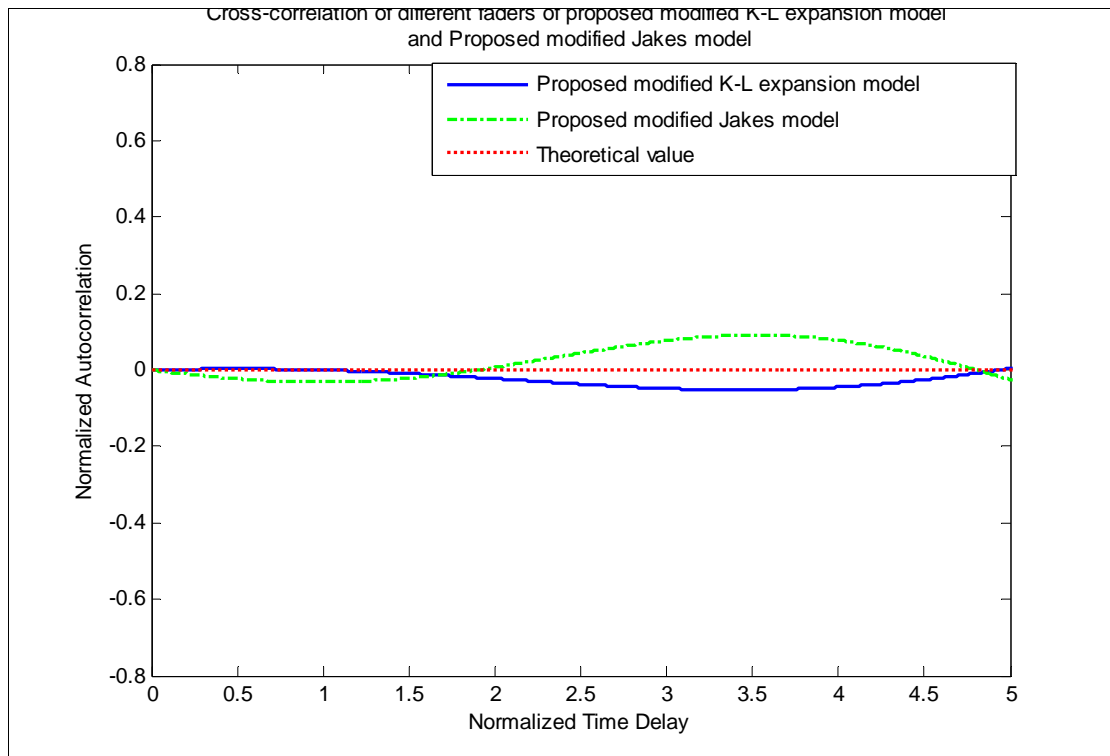
Figure 3-11: Cross-correlation functions of proposed modified Jakes model and proposed modified K-L expansion model

3.4.4 Degree of Chebyshev Approximation

Chebyshev approximation is useful for reducing the computational complexity because of its iterative characteristics. The degree choice for fitting the eigenfunctions is the major factor in effecting precision. In this section, we will discuss the tradeoff between the computational complexity and the precision. Choosing the most complicated eigenfunction of real part and imaginary part respectively, the degree of polynomial curve fitting can be decided under permitting mean square error.

For $N = 2$, Figure 3-12 and Figure 3-13 show the polynomial curve fitting for the real component of the 6-th eigenfunction and the imaginary component of the 5-th eigenfunction, respectively. It is shown the relationship of mean-square-error and the degree of curve fitting. As shown in Table 3-3 and Table 3-4, more degree of polynomial will have higher precision for curve fitting. If we would like to have

$\text{MSE} < 10^{-3}$, the least degree of real part of the 6-th eigenfunction should select $(2N + 6)$, as well as the least degree of imaginary part of the 5th eigenfunction should select $(2N + 5)$.
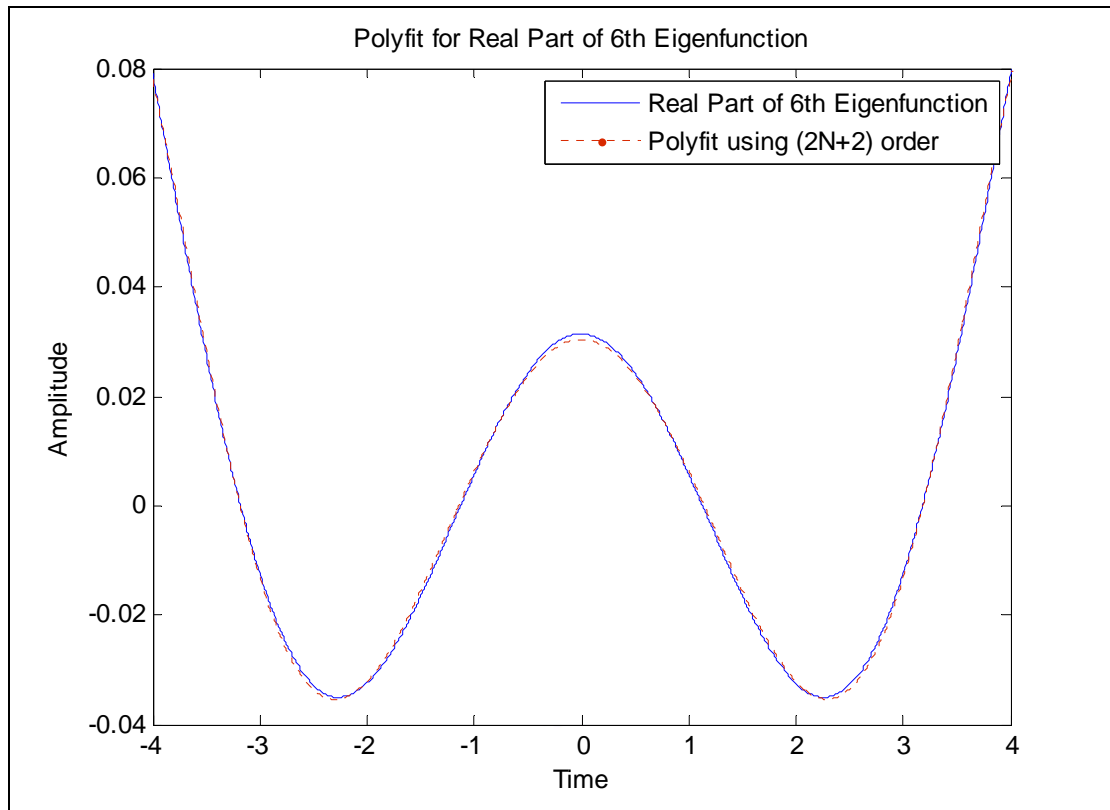
Figure 3-12: Polynomial curve fitting for real part of the 6th eigenfunction ($N = 2$)
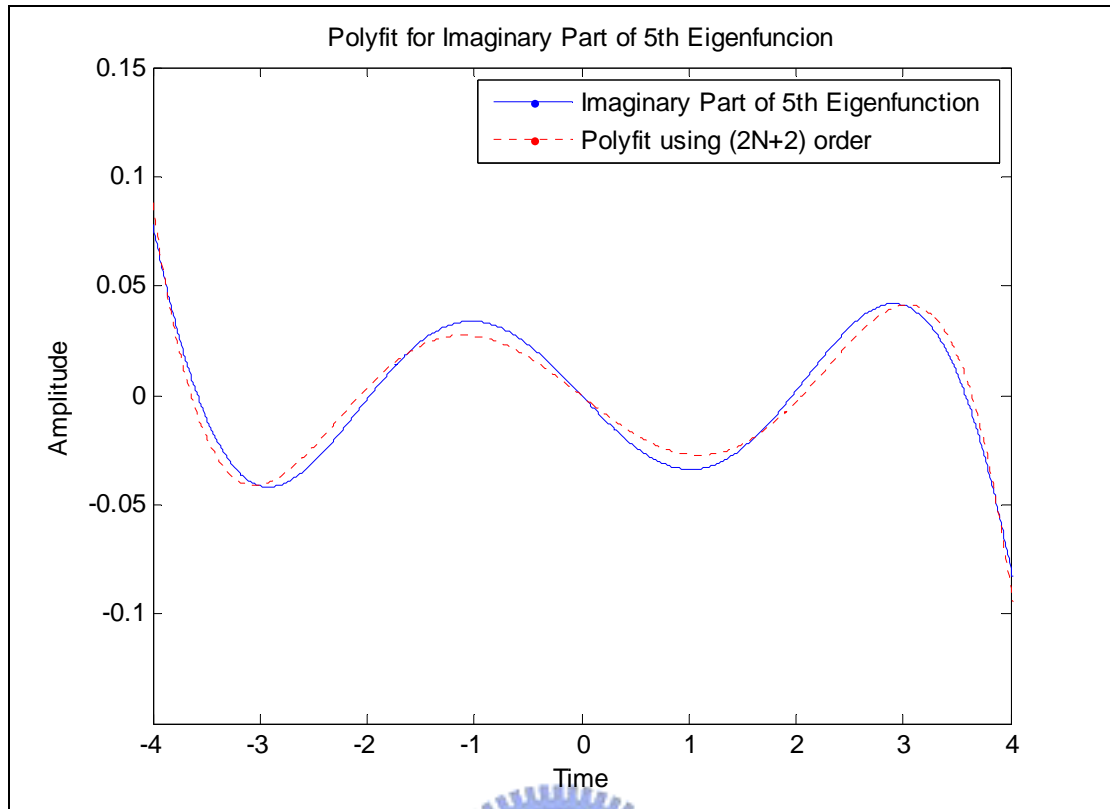
Figure 3-13: Polynomial curve fitting for imaginary part of the 5th eigenfunction
($N = 2$)

Table 3-3: Polynomial curve fitting of real part of the 6th eigenfunction and its corresponding mean square error ($N = 2$)

Degree MSE	$L = (2N+2)$	$L = (2N+4)$	$L = (2N+6)$
MSE of Real Part	0.0257	0.0014	0.0001

Table 3-4: Polynomial curve fitting of imaginary part of the 5th eigenfunction and its corresponding mean square error ($N = 2$)

Degree MSE	$L = (2N+1)$	$L = (2N+3)$	$L = (2N+5)$
MSE of Imag. Part	0.1832	0.0145	0.0007

3.5 Summary

In Chapter3, we propose the modified models for simulating Rayleigh fading channels. In the respect of sum-of-sinusoids method, Wu model is selected because of its less computational complexity. Furthermore, the proposed modified Jakes model improves the accuracy of Wu model but requires almost computational complexity. The MSE of the proposed method will be lower because of the independent initial random phase.

However, we are not satisfied with the performance of proposed modified Jakes model. K-L expansion method is considered to modify it. We consider the K-L expansion model to be more complete, and compare it with the proposed model using the concept of sum-of-sinusoids. From the simulation results, the proposed modified method using the concept of K-L expansion is better. In terms of statistic properties, autocorrelation and cross-correlation functions of proposed modified K-L expansion model are relatively close to the desired ones. From the viewpoint of computational complexity, our proposed modified K-L expansion model costs less run-time and needs more flexibility.

In order to reduce more computational complexity, we replace the eigenfunctions of proposed modified K-L expansion model with Chebyshev polynomials and determined weighting matrix. Under the acceptable MSE, the degree of Chebyshev polynomial can be determined. Because of the recursive polynomials and determined weighting matrix, the requirement of computational complexity is less.

The above analysis is under the flat fading environment. In Chapter 4, the proposed Rayleigh fading simulator will extend to the wideband system and MIMO channel.

Chapter 4

Rayleigh Fading Channel Simulators for MIMO System

The channel capacity of a communications link can be greatly increased by deploying multiple transmit and multiple receive antennas. Multiple-input multiple-output (MIMO) capacity were developed based on complex Gaussian independent identically distributed (i.i.d.) channel matrices with additive white Gaussian noise. As well as the performance of realistic receivers, the theoretical capacity depends on the statistical properties of the channel. For realistic thinking of MIMO capacity and algorithms, channel effects such as frequency selective, time variation, spatial and temporal correlations need to be considered.

MIMO channel models can be divided into three classes: ray-tracing, scattering, and correlation models [27]. In the ray-tracing approach, free-space propagation, reflection, diffraction, and scattering are modeled to follow each propagation path through the channel. In the correlation model, MIMO channels are created by multiplying a complex Gaussian i.i.d. matrix by the square roots of the correlation matrices at the receiver and the transmitter [28]-[31]. The scattering model assumes a particular distribution of the scatters and generates channel realizations based on the interaction of scatters and plane wavefronts [32]-[35].

The MIMO communication system is now quite popular, the request for models that simulate the channel effects in MIMO systems becomes more and more important. For fast development and real-time prototyping of MIMO communication systems, a real-time MIMO channel simulator can be very attractive [36]. The greatest challenge in implementing a real-time MIMO channel system is the large number of independent required Rayleigh faders by using Jakes model. To solve this problem, the proposed Rayleigh fading model using K-L expansion method can have less hardware cost. We will discuss how to extend our proposed Rayleigh fader to MIMO system in the following sections.

4.1 Spatial Channel Model for Mobile Wireless Applications

Spatial channel model (SCM) is adopted by third Generation Partnership Project (3GPP), which is applied for fixed and mobile MIMO wireless communications [37]. The categories of the channel environments are three scenarios: suburban macro-cell (approximated 3km distance BS to BS), urban macro-cell (approximated 3km distance BS to BS), and urban micro-cell (less than 1km distance BS to BS). For urban and suburban macro-cell environments, the cellular radius is 1-6 km and the BS antennas are above rooftop height, which is about 10-80 m and the mean height is 32m. The speed of mobility is 0-250 km/hr. For urban micro-cell environment, the cellular radius is 0.3-0.5 km and the BS antennas are at rooftop height, which has the mean height is about 12.5m. The speed of mobility is 0-120 km/hr. There is a notice that the urban micro-cell environment is relatively sensible for antenna height and scattering environment.

For system level simulation purposes, the fast fading per-path will be evolved in time, although bulk parameters including angle spread (AS), delay spread (DS), lognormal shadow fading (SF), and MS location will remain fixed during its evaluation.

The received signal at MS consists of N time-delayed multipath copies of the transmitted signal. Each scenario is characterized by a set of channel parameters. Each path consists of M subpaths. The parameters are shown in Figure 4-1. The following definitions are used :

v : MS velocity vector.

θ_v : Angle of the velocity with respect to the MS broadside: $\theta_v = \arg(v)$.

Ω_{BS} : BS antenna array orientation, defined as the difference between the

broadside of the BS array and the absolute North (N) reference direction.

Ω_{MS} : MS antenna array orientation, defined as the difference between the broadside of the MS array and the absolute North reference direction.

θ_{BS} : LOS angle of departure (AoD) direction between the BS and MS, with respect to the broadside of the BS array.

θ_{MS} : Angle between the BS-MS LOS and the MS broadside.

$\delta_{n,AoD}$: AoD for the nth $(n = 1,...,N)$ path with respect to the LOS AoD $\theta_{0,BS}$.

$\delta_{n,AoA}$: Angle of arrival (AoA) for the nth $(n = 1,...,N)$ path with respect to the LOS AoA $\theta_{0,MS}$.

$\Delta_{n,m,AoD}$: Offset for the mth $(m = 1,...,M)$ subpath of the nth path with respect to $\delta_{n,AoD}$.

$\Delta_{n,m,AoA}$: Offset for the mth $(m = 1,...,M)$ subpath of the nth path with respect to $\delta_{n,AoA}$.

$\theta_{n,m,AoD}$: Absolute AoD for the mth $(m = 1,...,M)$ subpath of the nth path at the BS with respect to the BS broadside.

$\theta_{n,m,AoA}$: Absolute AoA for the mth $(m = 1,...,M)$ subpath of the nth path at the MS with respect to the MS broadside
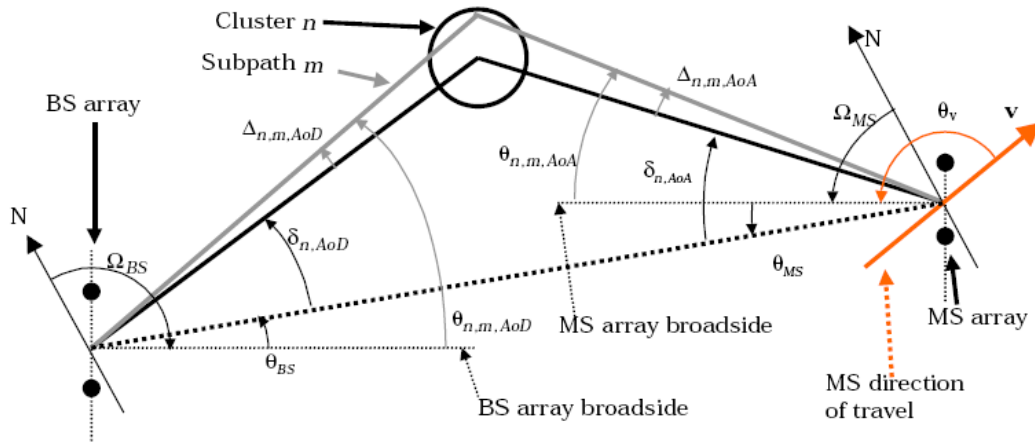
Figure 4-1: BS and MS angle parameters

4.2 Wideband Fading Channels for SISO System

The proposed Rayleigh fader simulator based on K-L expansion method can be extended to single-input single-output (SISO) system. It only needs to add the effects of multipath delay and fading gain as shown in Figure 4-2. Assuming there are M faders (taps) in SISO system, the mathematical formulation of Rayleigh fading channel simulator $r(t)$ for SISO system can be simply derived as:

$$r(t) = \frac{1}{E_0} \sum_{i=0}^{M-1} a_i \tilde{x}(t - \tau_i)$$

(4-1)

where $E_0 = \sqrt{\sum_{i=0}^{M-1} \alpha_i^2}$ is used to normal the signal power to unity, $\tilde{x}(t)$ denotes a single fader, a_i is the ith tap gain, and τ_i is the ith tap delay.

The autocorrelation function for the wideband fading channel needs be derived for verifying the accuracy. The autocorrelation of $r(t)$ is given by

$$E[r(t)r(t-\varepsilon)] = E\left[\frac{1}{E_0}\sum_{i=0}^{M-1}\alpha_i\tilde{x}(t-\tau_i)\cdot\frac{1}{E_0}\sum_{i=0}^{M-1}\alpha_j\tilde{x}(t-\tau_j-\varepsilon)\right]$$

$$(\text{if } i=j) \qquad = \frac{1}{E_0^2}\sum_{i=0}^{M-1}\alpha_i^2 E\left[\tilde{x}(t-\tau_i)\tilde{x}(t-\tau_i-\varepsilon)\right]$$

$$= \frac{1}{E_0^2}\sum_{i=0}^{M-1}\alpha_i^2\cdot J_0(w_M\varepsilon)$$

$$\left(\because E[\tilde{x}(t)\tilde{x}(t-\varepsilon)] = J_0(w_M\varepsilon)\right)$$

$$= J_0(w_M\varepsilon),$$

(4-2)

where ε is the time delay. The autocorrelation function is also the Bessel function of

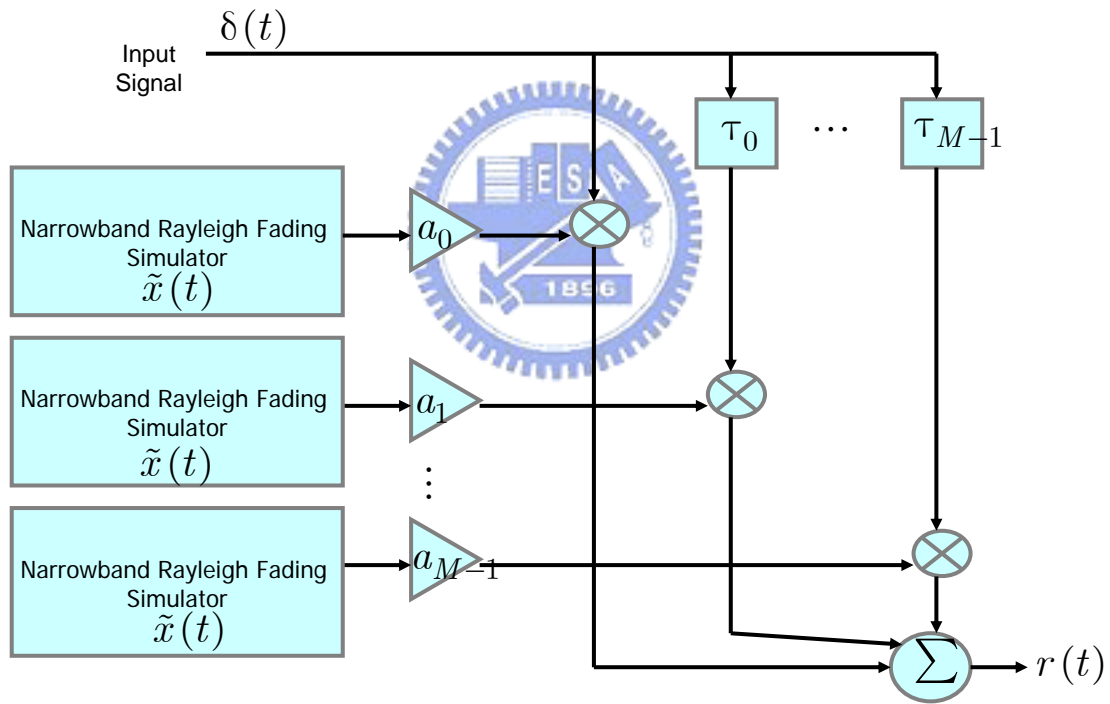delay, which is the same as that of a single fader.

Figure 4-2: Wideband Rayleigh fading channel simulator

4.3 Extension of Proposed Rayleigh Fader Simulator to MIMO System

According to TGn channel model, we suggest a realistic channel environment [38]. The channel environment combines the features of physical and non-physical MIMO channel models. There are L main links for MIMO channels, and each link corresponds to a wideband fading channel which is composed of M independent faders as shown in Figure 4-3. On the other hand, a circular disc (with radius R) of uniformly distributed scatters S is placed around the mobile unit. The channel parameter h_{nm} connecting transmit antenna m and receive antenna n is geometrically constrainted. The base station (BS) is assumed to be elevated and therefore not obstructed by local scattering, while the mobile station (MS) is surrounded by scatters. Figure 4-3 illustrates this scenario where T_x is the antenna elements at the BS, R_x is the antenna elements at the MS.

In the MIMO channel matrix H for each tap, at one instance of time, the models can be separated into a fixed (constant, LOS) matrix and a variable Rayleigh matrix. For the case of one-ring model there is only the Rayleigh matrix part since the LOS component is not included.

For a 2×2 MIMO system, the channel matrix H [39] is

$$H = \sqrt{P}\left(\sqrt{\frac{K}{K+1}}H_F + \sqrt{\frac{1}{K+1}}H_v\right)$$

$$= \sqrt{P}\left(\sqrt{\frac{K}{K+1}}\begin{bmatrix} e^{j\phi_{11}} & \frac{1}{\sqrt{10}}e^{j\phi_{12}} \\ \frac{1}{\sqrt{10}}e^{j\phi_{21}} & e^{j\phi_{22}} \end{bmatrix} + \sqrt{\frac{1}{K+1}}\begin{bmatrix} X_{11} & \frac{1}{\sqrt{2}}X_{12} \\ \frac{1}{\sqrt{2}}X_{21} & X_{22} \end{bmatrix}\right) \quad (4\text{-}3)$$

where the coefficients of the Rayleigh matrix H_v is defined as X_{nm} (n-th receiving and m-th transmitting antenna) which is correlated zero-mean complex Gaussian random variable with unit variance, $\exp(j\phi_{nm})$ is the element of fixed

matrix H_F, K is the Rician K-factor, and P is the power of each delay tap.

In order to correlate the X_{nm} elements of the matrix X, the Kronecker product of the transmit and receive correlation matrices is performed:

$$[X] = \left\{ \left[R_{T_X} \right] \otimes \left[R_{R_X} \right]^{1/2} \right\} \left[H_{iid} \right], \tag{4-4}$$

where R_{Tx} and R_{Rx} are the receive and transmit correlation matrices respectively, and H_{iid} is a vector of independent zero-mean complex Gaussian random variables with unit variance (i.e. the wideband fading signal).

The transmit and receive correlation matrices are expressed as

$$R_{Tx} = \begin{bmatrix} 1 & \rho^*_{Tx12} \\ \rho_{Tx21} & 1 \end{bmatrix} \quad \text{and} \quad R_{Rx} = \begin{bmatrix} 1 & \rho^*_{Rx12} \\ \rho_{Rx21} & 1 \end{bmatrix}, \tag{4-5}$$

where ρ_{Txnm} is the complex correlation coefficient between n-th and m-th transmitting antennas, and ρ_{Rxnm} is the complex correlation coefficients between m-th and n-th receiving antennas. According to the above mentioned, the relationships can be reformulated [40].

Letting the MIMO system dimension be $M_T \times M_R$, the general signal model for this system can be given by

$$r = Hs + n, \tag{4-6}$$

where r denotes the $M_R \times 1$ receive signal vector, s is the $M_T \times 1$ transmit signal vector, n is the $M_R \times 1$ noise vector, and H is the channel matrix with size $M_R \times M_T$. The complete channel matrix H of Kronecker model can be decomposed as

$$H = R_r^{1/2} H_{iid} R_t^{1/2}, \tag{4-7}$$

where the $M_R \times M_R$ receive covariance matrix R_r and the $M_T \times M_T$ transmit covariance matrix R_t are positive semi-definite Hermitian matrices. H_{iid} is the $M_R \times M_T$ identically independent distributed complex Gaussian matrix, in which all

elements are mutually independent Rayleigh fading waveforms, thus $M_R \times M_T$ mutually independent Rayleigh faders are needed. The coefficients ρ in R_r and R_t matrices could be derived as follows [41]:

$$
\begin{aligned}
\rho &= \int_{-\pi}^{\pi} \exp\left\{-j\vec{d} \cdot \vec{k}\right\} P(\phi)\, d\phi \\
&= \int_{-\pi}^{\pi} \cos(D\sin\phi) P(\phi)\, d\phi + j \int_{-\pi}^{\pi} \sin(D\sin\phi) P(\phi)\, d\phi,
\end{aligned}
\tag{4-8}
$$

where $\vec{d}$ is the position vector of the Tx/Rx antenna array, $\vec{k}$ is the directional vector with main signal propagation, D is the normalized distance between adjacent antennas of the Tx/Rx antenna array, and $P(\phi)$ is the power azimuth spectrum (PAS) for each antenna in Tx/Rx.

Using the notations of [42], with d/λ standing for the normalized distance between elements, where d and λ are the element spacing and the wavelength, respectively. The normalized distance between adjacent antenna of the Tx/Rx antenna array $D = (2\pi d)/\lambda$ like Figure 4-4, one can easily derives the cross-correlation function between the real and imaginary parts of the complex baseband signals received at two omni-directional antennas separated by the distance d.

The evolution of the correlation coefficients as a function of the distance between the antenna elements mostly depends on the PAS and on the radiation pattern of the antenna elements [43]. The PAS distribution can be divided into three types of different distributions: Uniform, Truncated Gaussian [44], and Truncated Laplacian [45]. Furthermore, Truncated Laplacian distribution is proposed as the best fit to measurement results in urban and rural areas. For the channel environment in this thesis, Truncated Laplacian distribution is the most suitable.

A. Uniform PAS

Consider the multi-cluster uniform PAS modeled as

$$
PAS_U(\phi) = \sum_{n=1}^{N_c} Q_{U,k} \left\{ \varepsilon\left[\phi - \left(\phi_{0,k} - \triangle\phi_k\right)\right] - \varepsilon\left[\phi - \left(\phi_{0,k} + \triangle\phi_k\right)\right] \right\}
\tag{4-9}
$$

where $\varepsilon(\phi)$ denotes the step function and N_c is the number of clusters.

The first step is to normalize the PAS such that it can be thought as a probability distribution. The constants $Q_{U,k}$ are derived such that $PAS_U(\phi)$ fulfills the requirements of a probability distribution function:

$$\int_{-\pi}^{\pi} PAS_U(\phi)d\phi = \sum_{k=1}^{N_c} \int_{\phi_{0,k}-\triangle\phi_k}^{\phi_{0,k}+\triangle\phi_k} Q_{U,k}d\phi = 1 \tag{4-10}$$

where $\triangle\phi$ is the half-domain definition of the PAS (domain is assumed symmetric). Equation 4-9 leads to $2\sum_{k=1}^{N_c} Q_{U,k}\triangle\phi_k = 1$.

The cross-correlation function between the real parts, which is as the same as the one derived for the imaginary parts, which is written as follows:

$$R_{XX}(D) = R_{YY}(D) \tag{4-11}$$

The autocorrelation function of the real-part is

$$R_{XX}(D) = \int_{-\pi}^{\pi} \cos(D\sin\phi)PAS(\phi)\,d\phi$$
$$= J_0(D) + 4\sum_{k=1}^{N_c} Q_{U,k} \sum_{m=1}^{\infty} \frac{J_{2m}(D)}{2m}\cos(2m\phi_{0,k})\sin(2m\triangle\phi_k) \tag{4-12}$$

where J_m is the Bessel function of the first kind at m-th order.

The cross-correlation function between real and imaginary part is

$$R_{XY,U}(D) = \int_{-\pi}^{\pi} \sin(D\sin\phi)PAS(\phi)\,d\phi$$
$$= 4\sum_{k=1}^{N_c} Q_{U,k} \sum_{m=0}^{\infty} \frac{J_{(2m+1)}(D)}{(2m+1)}\sin\big[(2m+1)\phi_{0,k}\big]\sin\big[(2m+1)\triangle\phi_k\big] \tag{4-13}$$

From these resolutions, both field $\rho_f(D)$ and envelope $\rho_e(D)$ correlation coefficients are defined as

$$\rho_e(D) \triangleq \big|\rho_f(D)\big|^2 \triangleq \big|R_{XX}(D) + jR_{XY}(D)\big|^2 \tag{4-14}$$

B. Truncated Gaussian PAS

Truncated Gaussian PAS model is defined as:

$$PAS_G(\phi) = \sum_{k=1}^{N_c} \frac{Q_{G,k}}{\sigma_{G,k}\sqrt{2\pi}} \exp\left[-\frac{(\phi-\phi_0)^2}{2\sigma_{G,k}^2}\right]$$
$$\left\{\varepsilon\left[\phi-(\phi_{0,k}-\triangle\phi_k)\right]-\varepsilon\left[\phi-(\phi_{0,k}+\triangle\phi_k)\right]\right\} \tag{4-15}$$

The normalization constant $Q_{U,k}$ are derived such that

$$\sum_{k=m}^{N_c} Q_{G,k}\, erf\left(\frac{\triangle\phi}{\sigma_{G,k}\sqrt{2}}\right) = 1 \tag{4-16}$$

Using above definition and normalization condition, the cross-correlation functions are easily derived, which can be given by

$$R_{XX,G}(D) = J_0(D) + \sum_{k=1}^{N_c} Q_{G,k} \sum_{m=1}^{\infty} J_{2m}(D)\cos(2m\phi_{0,k})\exp(-2\sigma_{G,k}^2 m^2)$$
$$\Re\left[erf\left(\frac{\triangle\phi_k}{\sigma_{G,k}\sqrt{2}} - jm\sigma_{G,k}\sqrt{2}\right) - erf\left(-\frac{\triangle\phi_k}{\sigma_{G,k}\sqrt{2}} - jm\sigma_{G,k}\sqrt{2}\right)\right] \tag{4-17}$$

$$R_{XY,G}(D) = \sum_{k=1}^{N_c} Q_{G,k} \sum_{m=1}^{\infty} J_{(2m+1)}(D)\sin\left[(2m+1)\phi_{0,k}\right]\exp\left[-2\sigma_{G,k}^2\left(m+\frac{1}{2}\right)^2\right]$$
$$\Re\left[erf\left(\frac{\triangle\phi_k}{\sigma_{G,k}\sqrt{2}} - j\sigma_{G,k}\sqrt{2}\left(m+\frac{1}{2}\right)\right) - erf\left(-\frac{\triangle\phi_k}{\sigma_{G,k}\sqrt{2}} - j\sigma_{G,k}\sqrt{2}\left(m+\frac{1}{2}\right)\right)\right]$$
$$\tag{4-18}$$

C. Truncated Laplacian PAS

Truncated Laplacian PAS model is defined as

$$PAS_L(\phi) = \sum_{k=1}^{N_c} \frac{Q_{L,k}}{\sigma_{L,k}\sqrt{2\pi}} \exp\left[-\frac{\sqrt{2}\,|\phi-\phi_{0,k}|}{\sigma_{L,k}^2}\right]$$
$$\left\{\varepsilon\left[\phi-\left(\phi_{0,k}-\triangle\phi_k\right)\right]-\varepsilon\left[\phi-\left(\phi_{0,k}+\triangle\phi_k\right)\right]\right\} \tag{4-19}$$

The normalization condition is given by

$$\sum_{k=m}^{N_c} Q_{L,k} \left[1 - \exp\left(\frac{\sqrt{2}\triangle\phi_k}{\sigma_{L,k}} \right) \right] = 1 \qquad (4\text{-}20)$$

As well as the cross-correlations is given by

$$R_{XX,L}(D) = J_0(D) + 4\sum_{k=1}^{N_c} \frac{Q_{L,k}}{\sigma_{L,k}\sqrt{2}} \sum_{m=1}^{\infty} \frac{J_{2m}(D)}{\left(\dfrac{\sqrt{2}}{\sigma_{L,k}} \right)^2 + (2m)^2} \cos\left(2m\phi_{0,k} \right)$$

$$\left[\left| \frac{\sqrt{2}}{\sigma_{L,k}} + \exp\left(-\frac{\triangle\phi_k\sqrt{2}}{\sigma_{L,k}} \right) \right| \left[2m\sin(2m\triangle\phi_k) \right. \right. \qquad (4\text{-}21)$$
$$\left. \left. - \frac{\sqrt{2}}{\sigma_{L,k}}\cos(2m\triangle\phi_k) \right] \right]$$

$$R_{XY,L}(D) = 4\sum_{k=1}^{N_c} \frac{Q_{L,k}}{\sigma_{L,k}\sqrt{2}} \sum_{m=1}^{\infty} \frac{J_{(2m+1)}(D)}{\left(\dfrac{\sqrt{2}}{\sigma_{L,k}} \right)^2 + (2m+1)^2} \sin\left[(2m+1)\phi_{0,k} \right]$$

$$\left[\left| \frac{\sqrt{2}}{\sigma_{L,k}} - \exp\left(-\frac{\triangle\phi_k\sqrt{2}}{\sigma_{L,k}} \right) \right| \left[(2m+1)\sin\left[(2m+1)\triangle\phi_k \right] \right. \right. \qquad (4\text{-}22)$$
$$\left. \left. + \frac{\sqrt{2}}{\sigma_{L,k}}\cos\left[(2m+1)\triangle\phi_k \right] \right] \right]$$
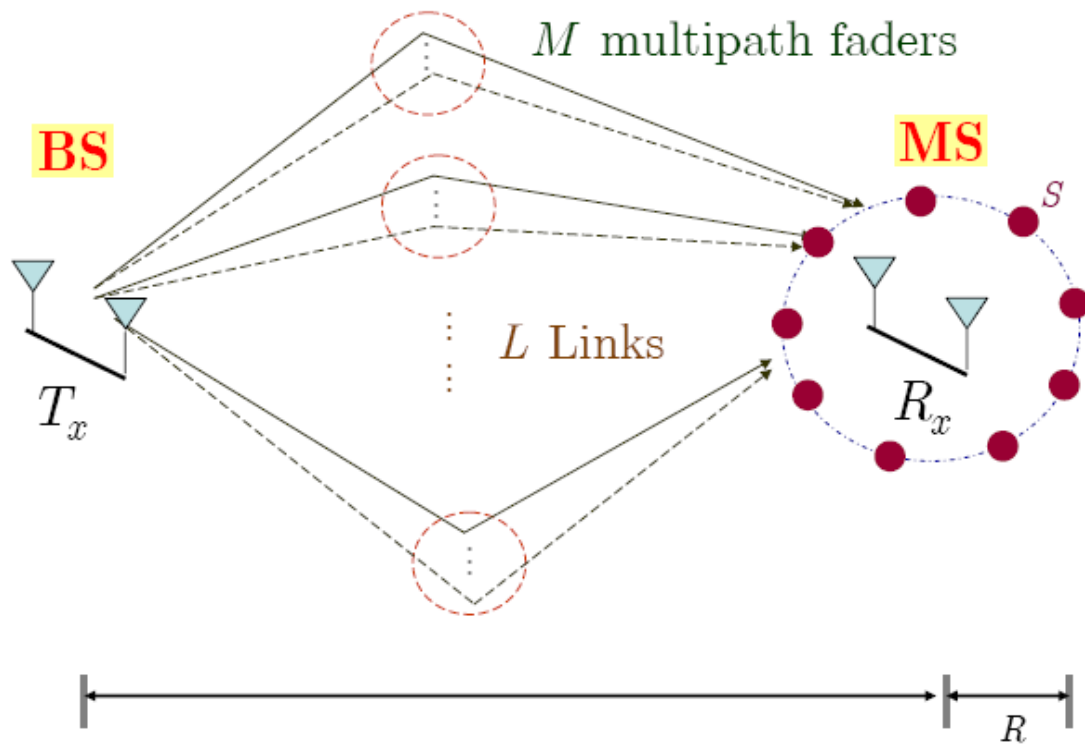
Figure 4-3: Propagation channel model for 2 X 2 MIMO system
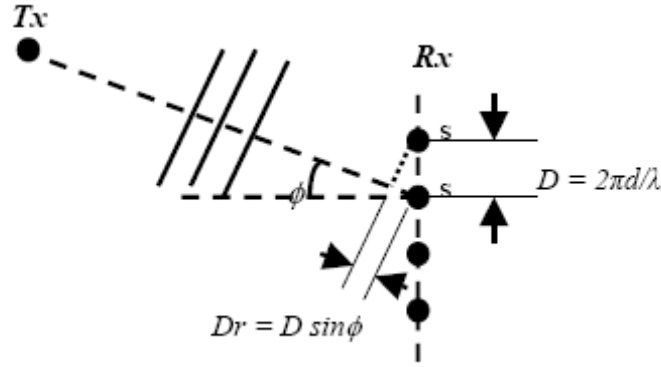
Figure 4-4: Impinging waves from T_X to R_X

4.4 Computer Simulations

For the discussion of wideband fading channel for the SISO system, the fader follows the parameters setting of Section 3.4.3. We assume the number of faders $M = 6$, with tap gains $\{a_i\}$ given by

$$\begin{bmatrix} a_0 & a_1 & \cdots & a_{M-1} \end{bmatrix} = \begin{bmatrix} 0.5892 & 0.5661 & 0.3818 & 0.2926 & 0.2532 & 0.1921 \end{bmatrix},$$

and tap delays $\{\tau_i\}$ given by

$$\begin{bmatrix} \tau_0 & \tau_1 & \cdots & \tau_{M-1} \end{bmatrix} = \begin{bmatrix} 0 & 1/S & \cdots & 5/S \end{bmatrix},$$

where S is the symbol rate.

Figure 4-5 shows the autocorrelation of a wideband system for SISO. We can see it can approach the desired statistical value. However, the accuracy of wideband fading channel is not as good as that of narrowband fading channel, because the random variable for each fader will not be completely independent in the simulation. Thus, different faders are not absolutely independent.

For the discussion of MIMO system, we set the transmit antenna spacing $\lambda_T = 4\lambda$ and the receive antenna spacing $\lambda_R = 0.5\lambda$, where λ is the wavelength. The local scatters uniformly surround receive antennas at BS. For 2×2 MIMO

channel, there are four main links ($L = 4$) and each link is composed of six faders ($M = 6$), so there are twenty-four independent faders in the channel.

First to discuss the statistical characteristics of each link of 2×2 MIMO channel like Figure 4-6, the autocorrelation functions of different links shown in Figure 4-7 are similar. We can support different channel links for MIMO system is almost equivalent. The channel state for different links to transmit signal is fair.

Then, the statistical characteristics between all links of 2×2 MIMO channel are discussed. We bring up 6 different cases listed in Table 4-1. The cross-correlation functions of two channel links of distinctive cases are compared to verify the channel environment of transmitting signal. For Case A, it describes the cross-correlation function of h_{11} and h_{12}. Figure 4-8 shows the cross-correlation functions of Case A, Case B, Case C, and Case D. We compare the cross-correlation functions of distinctive cases. Case A and Case B have similar channel environments for transmitting signals. From the standpoint of received signal, the transmitted signal via h_{11} and h_{12} is identical with one via h_{21} and h_{22}. Whereas the transmitting antenna is apart from receive antennas, the receive antennas spacing is small enough for thinking receiving terminal as independent element. Therefore, Case A and Case B have similar channel environment. In the same way, the ratiocination of Case C and Case D can be obtained as above. Case C and Case D also have similar channel environment.

In terms of Case E and Case F, Figure 4-9 shows the cross-correlation functions of these two cases, and compares their statistical properties. Case E and Case F have similar statistical properties. Each receive antenna can be considered independent if the separation between transmitter and receiver are far enough. The transmitted signals via h_{11} and h_{22} is identical with ones via h_{12} and h_{21}. When the receive antenna spacing is smaller than the coherence distance 0.5λ, the signals received by

different antennas can be thought of experiencing the same fading. If the receiving antenna spacing is larger than the coherence distance, the received signals of different antennas experience different fading.
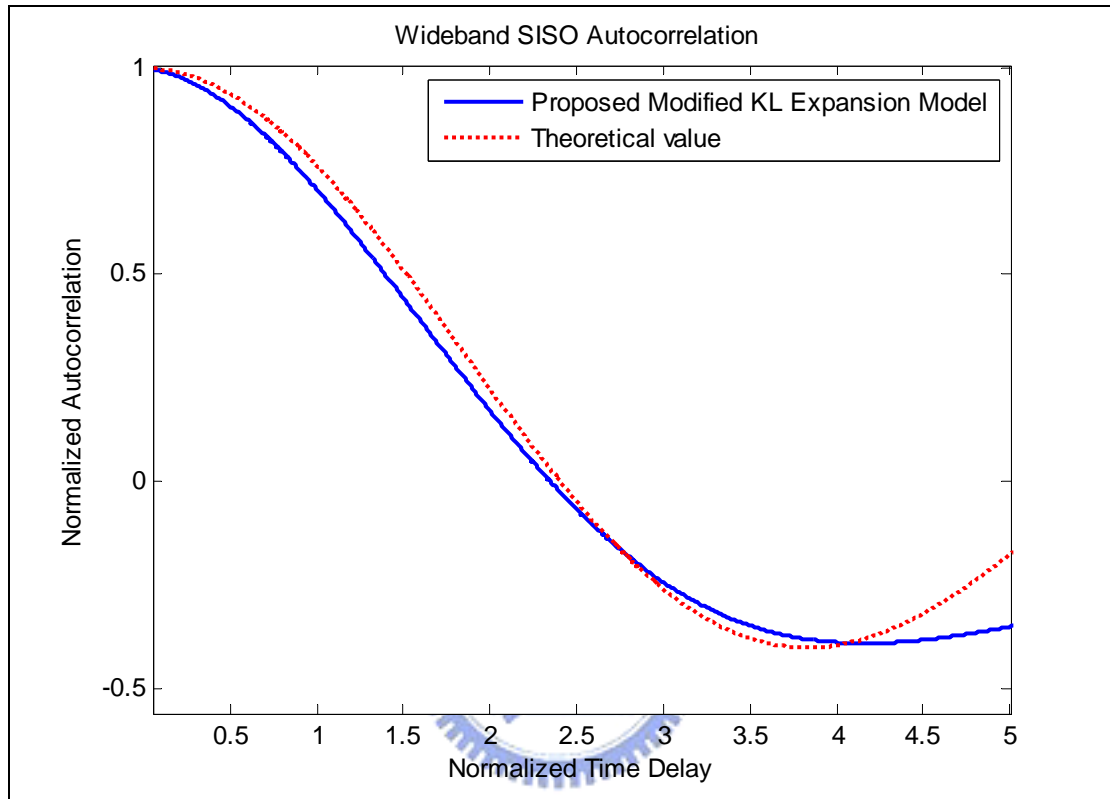

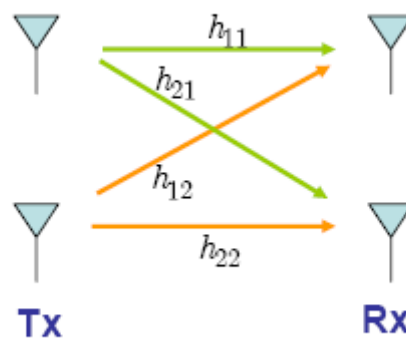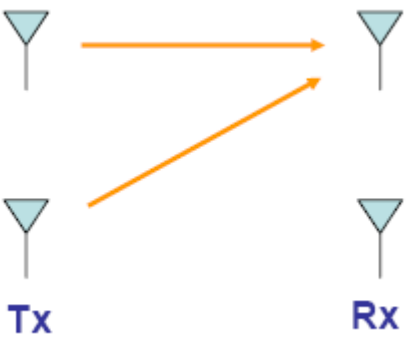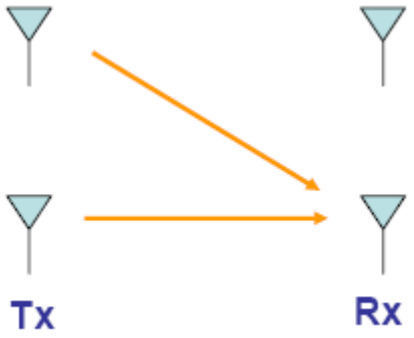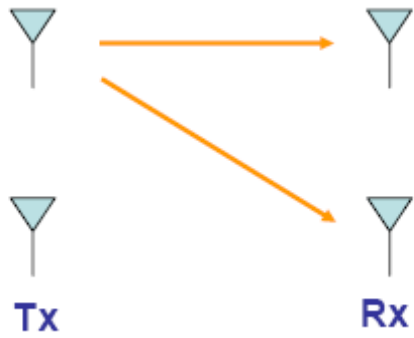**Figure 4-5:** Autocorrelation of wideband system for SISO ($M = 6$)
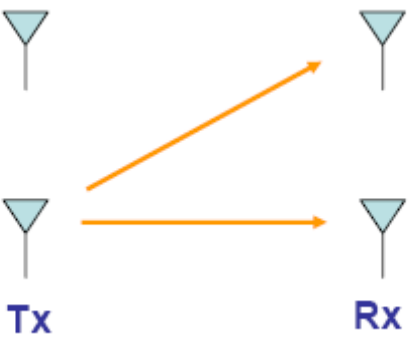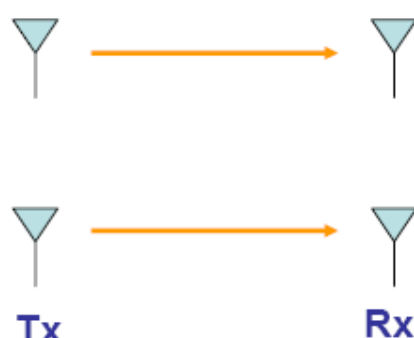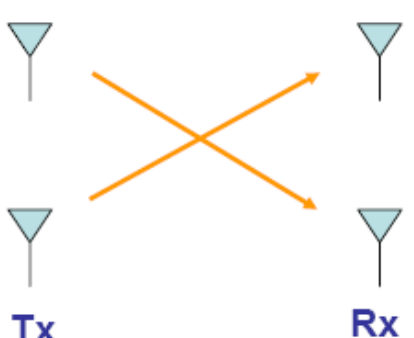
Figure 4-6: Links of 2×2 MIMO system

Table 4-1: Cross-correlation between different two links of 2×2 MIMO system

Case A	Case B
Case C	**Case D**
Case E	**Case F**

Figure 4-7: Autocorrelation for each link of 2×2 MIMO system

Figure 4-8: Cross-correlation functions of Case A, Case B, Case C, and Case D.

Figure 4-9: Cross-correlation functions of Case E and Case F.

4.5 Summary
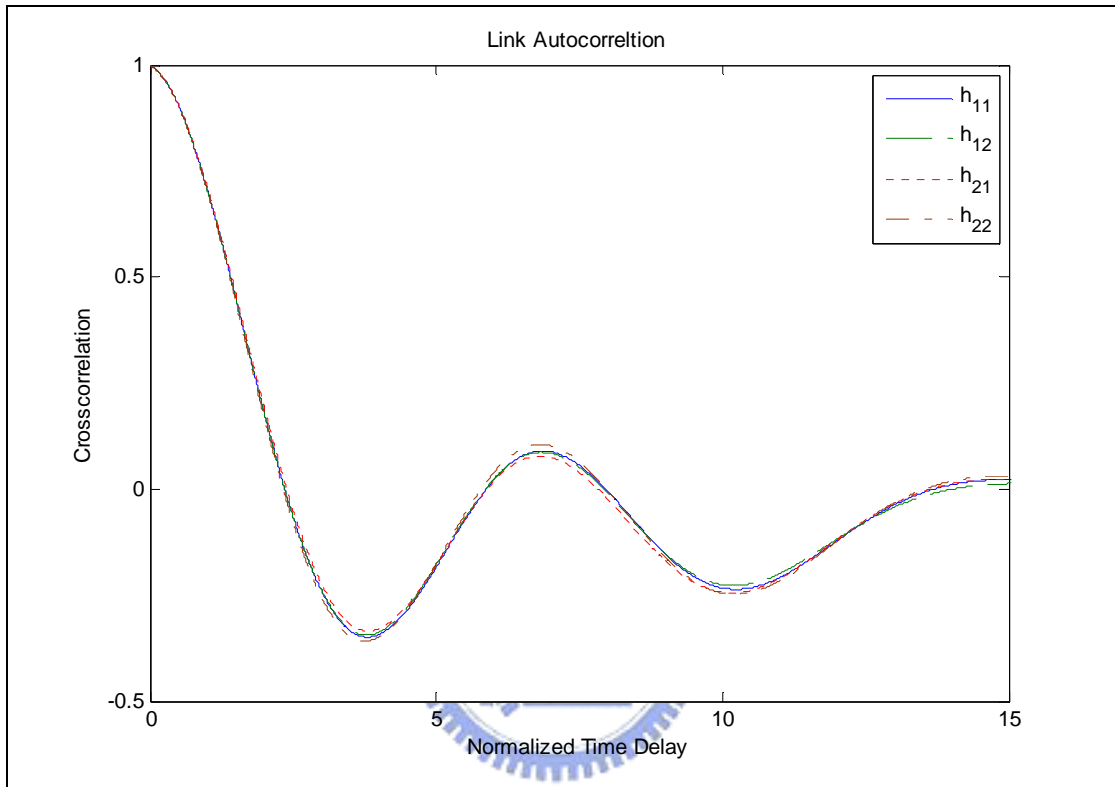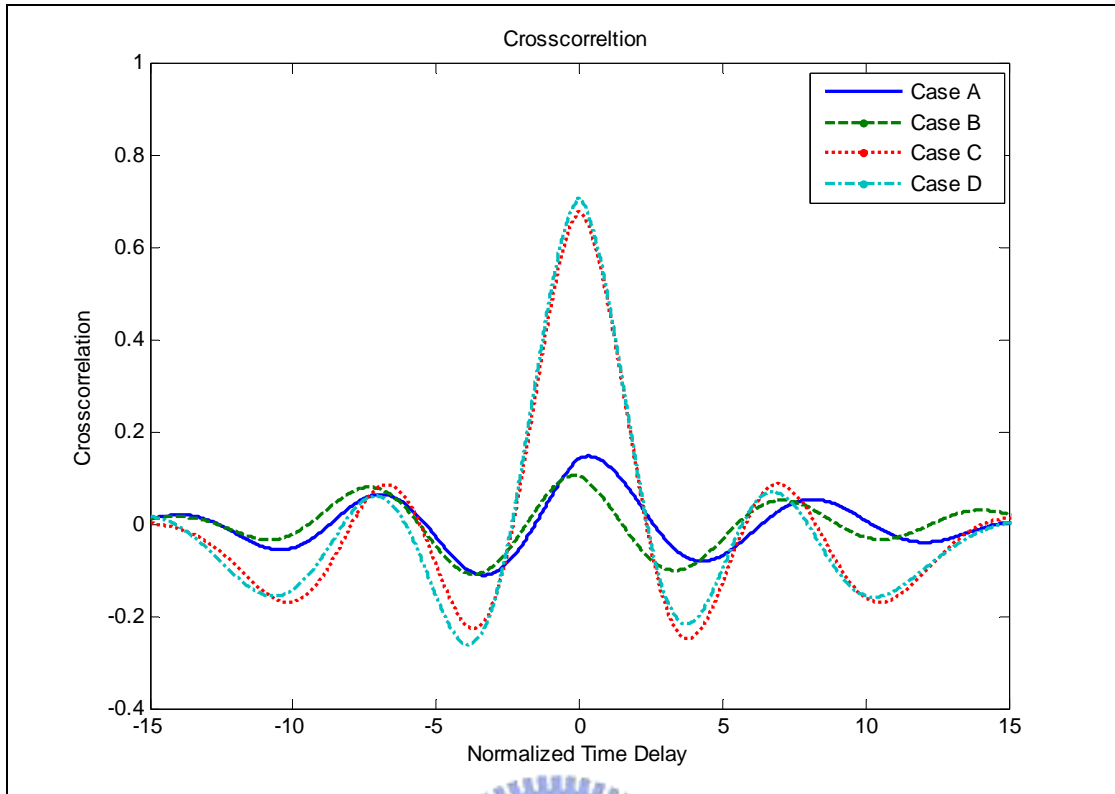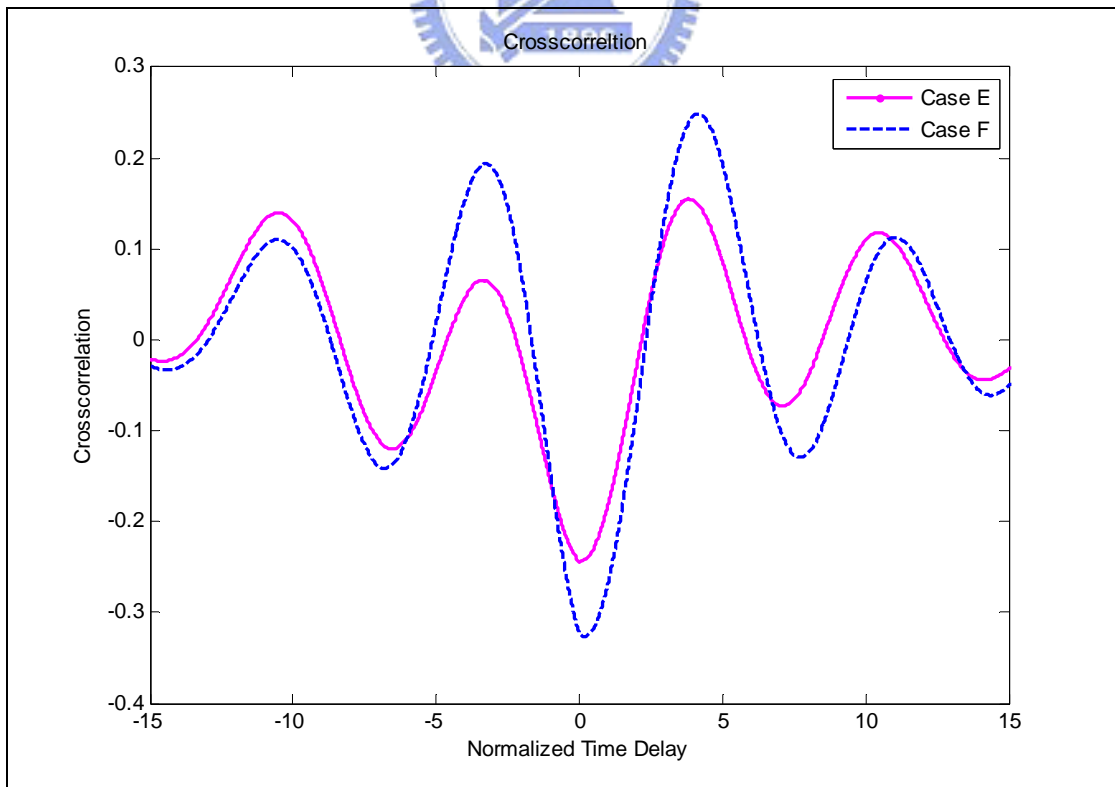
In this chapter, we use the proposed Rayleigh fader using the concept of K-L expansion method to expand to MIMO system. Observing the computer simulations, the statistical properties of the channel links conform with realistic channel environment. Unlike traditional method using sum-of-sinusoids, the advantages for using K-L expansion model are the flexible assignment of maximum Doppler frequency and less computational complexity.

Each fader can be assigned a different maximum Doppler frequency to construct the fading channel for a wideband system. However, Jakes model can just assign single maximum Doppler frequency. Therefore, our proposed Rayleigh fading channel simulator based on K-L expansion method can apply in variable velocity environment.

In terms of computational complexity, the analysis of computational loading has been discussed in Chapter 3. Because of less computational complexity of a single Rayleigh fader, the extended systems such as wideband and MIMO require lower computational complexity.

As above mentioned, the advantages of using the proposed fading channel based on K-L expansion method make real-time MIMO channel modeling simple to implement.

Chapter 5

Conclusion

In this thesis, we have propose two Rayleigh fading simulators based on Jakes model and K-L expansion model, respectively. According to the simulation results, the K-L expansion model is relatively more accurate and faster for simulating Rayleigh faders. We can assign adjustable maximum Doppler frequency to each fader for constructing frequency-selective fading. The proposed fading simulators are more flexible than traditional methods, thus facilitating efficient realization of real time MIMO channel modeling will also be more efficient.

In Chapter 2, the propagation channel models for mobile radio are introduced. Large and small scale fading is described, and small scale fading becomes the focus for later development. The theme of the thesis is then made clear to be on Rayleigh fading channel simulator development under the condition of WSSUS channels. In Chapter 3, we propose two Rayleigh fading simulators. First, the proposed Rayleigh fader based on sum-of-sinusoids has the same complexity with Wu model, but it can improve the statistical properties to be closer to the desired ones. Afterwards, the proposed fading simulator based on K-L expansion method is shown to have lower computational complexity. The proposed fading simulator based on K-L expansion method is more accurate and faster than the traditional method using sum-of-sinusoids. In Chapter 4, we extend the proposed Rayleigh fader based on the K-L expansion method to extend to MIMO channels.

To be more specific, the first proposed fading channel simulator is based on the modified Jakes model, which can improve the accuracy of Wu model with essentially the same computational complexity. The second simulator is based on the modified K-L expansion model, which has better accuracy and requires lower computational complexity than conventional ones. Further reduction in computational loading is achieved by substituting the basis functions with Chebyshev polynomials. In addition, the K-L expansion method is more flexible than traditional faders using Jakes model method, because a different maximum Doppler frequency can be assigned to each fader individually. Owing to these advantages, we extend proposed K-L expansion based simulator to MIMO channels. According to simulation results, the developed MIMO simulator meets well the requirement of realistic channel environments.

There are some future works worthy of further research. First, when realizing the fading simulator, fractional symbol rate is usually required for the tap delay. However, fractional tap delay is hard to implement in practice. Second, how to implement a great deal of uncorrelated random sequences efficiently is an interesting issue. Finally, the mobile-to-mobile local scattering environment can find increasing number of applications in futuristic intelligent transport systems, ad hoc mobile wireless networks, and relay-based cellular networks. Such mobile-to-mobile communication systems differ from the conventional cellular radio systems, where one terminal, the BS is stationary, and only the mobile station is moving. Efficient mobile-to-mobile Rayleigh fading channel simulators would be a topic of high interest in the future.

Bibliography

[1] M. Patzold, Mobile Fading Channels, N.Y.: Wiley, 2002.

[2] G. L. Stuber, Principle of Mobile Communication, Boston: Kluwer, 1996.

[3] M. Hata and T. Nagatsu, "Mobile location using signal strength measurements in cellular system," *IEEE Trans. Veh. Technol.*, vol. 29, pp. 245-251, May 1980.

[4] Y. Okumura, E. Ohmuri, T. Kawano, and K. Fukuda, "Field strength and its variability in VHF and UHF land mobile radio service," *Rev. of the ECL*, vol. 16, pp. 825-873, 1968.

[5] Cost 231 TD(91) 109, "1800 MHz mobile net planning based on 900 MHz measurements," 1991.

[6] W. C. Y. Lee, Mobile Cellular Telecommunications, 2nd ed. New York: McGraw-Hill, 1995.

[7] R. L. Bogusch, F. W. Guigliano, and D. L. Knepp, "Frequency-selective scintillation effects and decision feedback equation in high data-rate satellite links," *Proc. IEEE*, vol. 71, no. 6, pp.754-767, June 1983.

[8] T. S. Rappaport, Wireless Communications Principles and Practice. New York: Prentice Hall, 1996.

[9] J. H. Winters, J. S. Salz, and R. D. Gitlin, " The impact of antenna diversity on the capacity of wireless communication systems," *IEEE Trans. Commun.*, vol. 42, no. 2/3/4, pp.1740-1751, Feb./Mar./April 1994.

[10] T. S. Rappaport, Wireless Communications, CH 3 and 4, Upper Sadle River, NJ: Prentice Hall, 1996.

[11] B. Sklar, Digital Communications: Fundamentals and Applications, CH. 6, Eng lewood Cliffs, NJ: Prentice Hall, 1988.

[12] P. Bello, "Characterization of random time-variant linear channels," *IEEE Trans. Commun.*, vol.11, pp.360-393, Dec. 1963.

[13] T. S. Rappaport, Wireless Communications Principles and Practice, 2nd ed. Prentice Hall PTR, 2002.

[14] K.W. Yip and T. S. Ng, "Karhunen-Loeve expansion of the WSSUS channel output and its application of efficient simulation," *IEEE J. Select. Areas Commun.,* vol.15, pp. 640-646, May 1997.

[15] C. Komninakis, "A fast and accurate Rayleigh fading simulator," in *IEEE GLOBECOM 2003,* vol.6, El Segundo, CA, Dec. 1-5, 2003, pp. 3306-3310.

[16] S. A. Fechtel, "A novel approach to modeling and efficient simulation of frequency-selective fading radio channels," *IEEE J. Select. Areas Comm.,* vol. 11, no.3, pp. 422–431, Apr. 1993.

[17] R. H. Clarke, "A statistical theory of mobile-radio reception," *Bell Syst. Tech. J.*, pp. 957-1000, July-Aug. 1968.

[18] W. C. Jakes, Microwave Mobile Communications, 2nd ed. Piscataway, NJ: Wiley-IEEE Press, 1994.

[19] A. G. Zajic and G. L. Stuber, "Efficient simulation of Rayleigh fading with enhanced de-correlation properties," *IEEE Trans. Wireless Commun.*, vol. 5, no. 7, pp. 1866-1875, July 2006.

[20] M. F. Pop and N. C. Bealieu, "Limitations of sum-of-sinusoids fading channel simulators," *IEEE Trans. Commun.*, vol. 49, no. 4, pp. 699-708, Apr. 2001.

[21] Y. X. Li and X. Huang, "The simulation of independent Rayleigh faders," *IEEE Trans. Commun.*, vol. 50, no. 9, pp. 1503-1514, Sep. 2002.

[22] P. Dent, G. E. Bottomley, and T. Croft, "Jakes fading model revisited," *IEEE Electron. Lett.*, vol. 29, no. 23, pp. 1162-1163, June 1993.

[23] Z. Wu, "Model of independent Rayleigh faders," *IEEE Electron. Lett.*, vol. 40, no. 15, pp. 949-951, July 2004.

[24] Y. R. Zheng and C. Xiao, "Simulation models with correct statistical properties for Rayleigh fading channels," *IEEE Trans. Commun.*, vol. 51, no. 6, pp.920-928, June 2003.

[25] M. Visintin, "Karhunen-Loeve expansion of a fast Rayleigh fading process," *IEEE Electron. Lett.*, vol. 32, no. 18, pp. 1712-1713, Aug. 1996.

[26] J. K. Hwang, K. H. Lin, J. D. Li, and J. H. Deng, "Fast FPGA prototyping of a multipath fading channel emulator via high-level design," *IEEE ISCIT 2007*, vol. 10, Sydney, NSW, Oct. 17-19, 2007, pp. 168-171.

[27] H. Xu, D. Chizhik, H. Huang, and R. Valenzuela, "A generalized space-time multiple-input multiple-output (MIMO) channel model," *IEEE Trans. Commun.*, vol. 3, no. 3, pp. 966-975, May 2004.

[28] D. Chizhik, F. Rashid-Farrokhi, J. Ling, and A. Lozano, "Effects of antenna separation on the capacity of BLAST in correlated channels," *IEEE Commun. Lett.*, vol. 4, no. 11, pp. 337-339, Nov. 2000.

[29] D. Gesbert, H. Bolcskei, D. Core, and A. Paulraj, "MIMO wireless channels: Capacity and performance prediction," in *IEEE Globecom 2000,* vol. 2, San Francisco, CA, Nov. 27-Dec. 1, 2000, pp. 1083-1084.

[30] K. I. Pedersen, J. B. Andersen, J. P. Kermoal, and P. Modensen, "A stochastic multiple-input multiple-output radio channel model for evaluation of space-time coding algorithms," in *IEEE VTC 2000*, vol. 2, Boston, MA, Sept. 24-28, 2000, pp.893-897.

[31] A. L. Moustakas, "Communication through a diffusive medium: Coherence and capacity," *Science*, vol. 287, no. 5451, pp. 287-290, Jan. 2000.

[32] L. Correia, Wireless Flexible Personalized Communications. New York: Wiley, 2001.

[33] M. Steinbauer, A. Molisch, and E. Bonek, "The double-directional radio channel," *IEEE Antennas Propagat. Mag.*, vol. 43, no. 4, pp. 51-63, Aug. 2001.

[34] R. M. Buehrer, S. Arunachalam, K. H. Wu, and A. Tonello, "Spatial channel model and measurements for IMT-2000 systems," in *IEEE VTC 2001*, vol. 1, Rhodes, Greece, May 6-9, 2001, pp. 342-346.

[35] D. Shiu, G. J. Foschini, M. J. Gans, and J. M. Kahn, "Fading correlation and its effect on the capacity of multielement antenna systems," *IEEE Trans. Commun.*, vol. 48, no. 3, pp. 502-513, Mar. 2000.

[36] C. H. Liao, T. P. Wang, and T. D. Chiueh, "A novel low-complexity Rayleigh fader for real-time channel modeling," in *IEEE ISCAS 2007*, vol. 10, New Orleans, LA, May 27-30, 2007, pp. 2602-2605.

[37] 3GPP TR 25.996, "Spatial channel model for multiple input multiple output (MIMO) simulations," v7.0.0, Jun. 2006.

[38] V. Ecreg et al., IEEE 802.11 document 03/940r4 "TGn channel model," May 2004.

[39] V. Ecreg, "Indoor MIMO WLAN channel models," IEEE 802.11-03/161r2, Sept. 2003.

[40] T. P. Wang, C. H. Liao, and T. D. Chiueh, "A real-time digital baseband MIMO channel emulation system," in *IEEE ISCAS 2007*, vol. 10, New Orleans, LA , May 27-30, 2007, pp. 2606-2609.

[41] X. Hao, D. Chizhik, H. Huang, and R. Valenzueka, "A generalized space-time multiple-input multiple-output (MIMO) channel model," *IEEE Trans. Wireless Communications*, vol. 3, no. 3, pp.966-975, May 2004.

[42] J. Salz and J. Winters, "Effect of fading correlation on adaptive arrays in digital mobile radio," *IEEE Trans. Veh. Technol.*, vol. 43, no. 4, pp. 1049-1057, Nov. 1994.

[43] L. Schumacher, K. I. Pedersen, and P. E. Mogensen, "From antenna spacings to theoretical capacities—Guidelines for simulating MIMO systems," in *Proc. 13th IEEE Int. Symp. Pers., Indoor, Mobile Radio Commun.*, vol. 2, Aalborg, Denmark, Sep. 15-18, 2002, pp. 587–592.

[44] F. Adachi, M. Feeny, A. Williamson, and J. Parsons, "Cross-correlation between the envelopes of 900 MHz signals received at a mobile radio base station site," *IEE Proceeding Pt. F.,* vol. 133, no. 6, pp. 506-512, Oct. 1986.

[45] K. I. Pedersen, P. E. Mogensen, and B. H. Fleury, "Spatial channel characteristics in outdoor environments and their impact on BS antenna system performance," *in Proceedings of IEEE Veh. Technol. Conference VTC 1998,* Ottawa, Canada, vol. 2, pp. 719-723, 1998.